BBA - Molecular Basis of Disease 1866 (2020) 165581

Contents lists available at ScienceDirect

BBA - Molecular Basis of Disease

journal homepage: www.elsevier.com/locate/bbadis

The imbalance between dynamic and stable microtubules underlies neurodegeneration induced by 2,5-hexanedione

Francesca V.M. Casagrande[a,*,1], Alida Amadeo[a,b], Daniele Cartelli[a,2], Alessandra M. Calogero[a], Debora Modena[a], Ilaria Costa[a,1], Francesca Cantele[a], Elisabetta Onelli[a], Alessandra Moscatelli[a], Miriam Ascagni[c], Gianni Pezzoli[d,3], Graziella Cappelletti[a,b,**,3]

[a] Department of Biosciences, University of Milan, Milan, Italy
[b] Center of Excellence on Neurodegenerative Diseases, University of Milan, Milan, Italy
[c] Unitech NOLIMITS, University of Milan, Milan, Italy
[d] Fondazione Grigioni per il Morbo di Parkinson, Milan, Italy

ARTICLE INFO

Keywords:
Parkinson's disease
2,5-Hexanedione
Microtubule dysfunction
Post-translational modified tubulins
Human skin fibroblasts
Neurodegeneration

ABSTRACT

Exposure to environmental toxins, including hydrocarbon solvents, increases the risk of developing Parkinson's disease. An emergent hypothesis considers microtubule dysfunction as one of the crucial events in triggering neuronal degeneration in Parkinson's disease. Here, we used 2,5-hexanedione (2,5-HD), the toxic metabolite of *n*-hexane, to analyse the early effects of toxin-induced neurodegeneration on the cytoskeleton in multiple model systems. In PC12 cells differentiated with nerve growth factor for 5 days, we found that 2,5-HD treatment affected all the cytoskeletal components. Moreover, we observed alterations in microtubule distribution and stability, in addition to the imbalance of post-translational modifications of α-tubulin. Similar defects were also found *in vivo* in 2,5-HD-intoxicated mice. Interestingly, we also found that 2,5-HD exposure induced significant changes in microtubule stability in human skin fibroblasts obtained from Parkinson's disease patients harbouring mutations in *PRKN* gene, whereas it was ineffective in healthy donor fibroblasts, suggesting that the genetic background may really make the difference in microtubule susceptibility to this environmental Parkinson's disease-related toxin. In conclusion, by showing the imbalance between dynamic and stable microtubules in hydrocarbon-induced parkinsonism, our data support the crucial role of microtubule defects in triggering neurodegeneration.

1. Introduction

The central pathological feature of Parkinson's disease (PD), the second most common neurodegenerative disorder worldwide, is mainly the selective degeneration of dopaminergic neurons in the *Substantia nigra pars compacta* projecting to the *Corpus striatum*, leading to severe striatal dopamine deficiency, which results in the typical movement disorders of parkinsonism [1,2]. For the vast majority of PD cases, the etiology remains unknown, even though both genetic and environmental factors are likely to be implicated [3,4]. Increasing evidence shows that parkinsonism can be induced by environmental toxins, such as pesticides and hydrocarbon solvents [5–7]. In detail, the correlation between *n*-hexane exposure and PD onset has been investigated mainly in humans following occupational exposure. The first case report suggesting that this volatile hydrocarbon might induce signs of parkinsonism dates back to 1989 [8]. Additional single case reports, as well as

Abbreviations: 2,5-HD, 2,5-hexanedione; CS, *Corpus striatum*; Dim, α-tubulin free dimers; MT, microtubule; NF, neurofilament; NF-L, neurofilament light protein; NF-M, neurofilament medium protein; NGF, nerve growth factor; NSF, nigro-striatal fibers; PD, Parkinson's disease; *PRKN*, Parkin gene; PTMs, post-translational modifications; SN, *Substantia nigra*; TH, tyrosine hydroxylase; α-Tub, α-tubulin; Ac Tub, acetylated tubulin; deTyr Tub, detyrosinated tubulin; Tyr Tub, tyrosinated tubulin

* Correspondence to: F.V.M. Casagrande, Imaging Technological Development Unit, IFOM – The FIRC Institute of Molecular Oncology, Via Adamello 16, Milano 20139, Italy.
** Correspondence to: G. Cappelletti, Department of Biosciences, University of Milan, Via Celoria 26, 20133 Milano, Italy.
E-mail addresses: francesca.casagrande@ifom.eu (F.V.M. Casagrande), graziella.cappelletti@unimi.it (G. Cappelletti).
[1] Present address: IFOM Foundation, The FIRC Institute of Molecular Oncology, Milan, Italy.
[2] Present address: Neuroalgology Unit, IRCCS Foundation, "Carlo Besta" Neurological Institute, Milan, Italy.
[3] Co-last authors.

https://doi.org/10.1016/j.bbadis.2019.165581
Received 30 May 2019; Received in revised form 17 September 2019; Accepted 12 October 2019
Available online 29 October 2019
0925-4439/

cohort and neuropathological studies [9–13], helped build up the hypothesis that hydrocarbon solvents may be involved in the etiopathogenesis of PD and might be associated with greater severity of motor symptoms. Intriguingly, meta-analysis revealed that exposure to pesticides or solvents is a risk factor for PD [14]. The search for a causal link between solvent exposure and neurodegeneration in PD requires the development of appropriate animal models. Although prolonged exposure to relatively high levels of certain aliphatic solvents, such as *n*-hexane and its toxic metabolite the γ-diketone 2,5-hexanedione (2,5-HD), causes dose-dependent neurodegeneration with clear prevalence of damage in the distal part of the nerve known as dying-back neuropathy [15–17], evidence indicates that *n*-hexane can also induce parkinsonism in animals. In detail, Pezzoli and colleagues demonstrated that *n*-hexane induces a specific dopamine depletion in rat *Corpus striatum* and behavioural defects [18,19]. More recently, Zhang and colleagues found neurodegeneration of nigrostriatal pathway in 2,5-HD-intoxicated mice with the loss of both nigral dopaminergic neurons and striatal dopaminergic terminals, thus supporting the causal effect of toxic exposure in PD etiology [20].

Given that 2,5-HD is the main toxic metabolite of *n*-hexane, there has been great interest in its levels and in the molecular mechanisms underlying its effects on the central nervous system. Both aging and PD have been associated with a reduction in the capacity to eliminate *n*-hexane, measured by blood and urine levels of its metabolites, an alteration which may also play a role in the pathogenesis of PD [21]. Notably, 2,5-HD has not only been detected in the urine and blood of workers with occupational exposure to *n*-hexane, but is also found at low concentrations in the general population [22–25]. Since in non-exposed persons only a minimal part of 2,5-HD could derive from *n*-hexane as an ubiquitous micropollutant, it may also be a product of intermediate metabolism in the human body [26], an assumption that makes the study of its molecular effects even more relevant. To date, the known molecular mechanism of action of 2,5-HD is its reaction with lysine amino groups of proteins forming pyrrole adducts, which probably undergo secondary oxidation, resulting in crosslinked proteins [17,27,28]. Neurofilament (NF) protein polymerization and crosslinking have been proposed as the cardinal lesion in aliphatic γ-diketone neuropathy, since NF accumulation leads to giant neurofilamentous axonal swellings and eventual degeneration in central and peripheral nervous system, typical of this kind of neuropathy [15,27]. The accumulation of NFs, however, does not appear to explain the onset of the distal axonal degeneration, which is likely to be a consequence of axonal transport impairment [29]. In addition, similar patterns of distal axonal degeneration were found in 2,5-HD neuropathy in wild-type and transgenic mice that do not express NFs [30]. Other potential targets of aliphatic and aromatic γ-diketones are microtubule (MT)-associated proteins [31] and MTs themselves [32].

Interestingly, MTs interact with some of the proteins mutated in PD, such as α-Synuclein [33], LRRK2 [34] and Parkin [35], and are affected by the action of PD toxins, such as 1-methyl-4-phenylpyridinium (MPP^+) [36] and rotenone [37]. Besides, due to the specific architecture of neurons, the functionality and survival of these cells are particularly dependent on intracellular transport sustained by MTs. The impairment of MTs might result in accumulation of damaged proteins and organelles forming the axonal swellings described in several neurodegenerative diseases [38,39]. A crucial regulator of MT functions is the so called “tubulin code”, which consists in post-translational modifications (PTMs) of tubulin, together with the expression of different α- and β-tubulin isotypes [40]. Additionally, neurons are an interesting case, as they are the only known cell type in which tubulin PTMs are strongly enriched in most cytosolic MTs and linked to neuronal diseases [41]. Under this light we investigated the changes in MT system after 2,5-HD treatment in a variety of cell lines, including nerve growth factor (NGF)-differentiated PC12 cells and human skin fibroblasts obtained from healthy donors and PD patients in addition to C57BL mice, to unravel the molecular mechanisms responsible for toxin-induced PD neurodegeneration. Here, we show the early impairment of MT stability in different models, thus suggesting that MT regulation could represent an interesting target for developing new and more efficient therapies.

2. Materials and methods

2.1. Maintenance and neural differentiation of PC12 cells

PC12 cells were maintained in RPMI 1640 (EuroClone, Pero, Italy) containing 10% horse serum (ECS0090D, EuroClone) and 5% fetal bovine serum (HyClone SH 30066, Thermo Fisher Scientific, Waltham, MA, USA), supplemented with 2 mM L-glutamine (EuroClone), penicillin/streptomycin both 100 μg/ml (EuroClone), at 37 °C in a humidified atmosphere and 5% CO_2. The medium was changed every 3–4 days. Cells were plated at $1.5 \times 10^4/cm^2$ onto poly-L-lysine (Sigma-Aldrich, St. Louis, MO)-coated cover glass in 35 mm petri dishes for immunofluorescence microscopy or directly onto poly-L-lysine-coated petri dishes for biochemical analysis. For neural differentiation, the cells were exposed to 50 ng/ml human β-NGF (PeproTeck, London, UK) in low serum medium (RPMI 1640 supplemented with 2% horse serum, 2 mM L-glutamine, penicillin/streptomycin). The differentiation medium was changed every 2–3 days with the fresh one. The PC12 cells were exposed to 2,5-HD (Sigma-Aldrich) at different concentrations after 5 days of differentiation with human β-NGF and analysed at different time points.

2.2. Ethic statement, generation and maintenance of human fibroblast cell lines

Primary fibroblasts were obtained by skin biopsies from 6 individuals. They included 3 healthy subjects as control group and 3 patients affected by PD, harbouring mutations in *PRKN* gene, whose characteristics are summarized in Table 2. All patients were examined by movement disorder neurologists and clinical diagnosis of PD was established according to the UK Parkinson Disease Society Brain Bank criteria [42]. The mutations on the *PRKN* gene were screened as previously described [43]. The study was approved by the local ethics committee (Istituti Clinici di Perfezionamento, July 13th 2010) and all participants gave written informed consent. Human fibroblasts were cultured in RPMI 1640 containing 15% foetal bovine serum (HyClone) supplemented with 2 mM L-glutamine, penicillin/streptomycin both 100 μg/ml (all from EuroClone) and 50 μM β-mercaptoethanol (Sigma-Aldrich), at 37 °C in a humidified atmosphere and 5% CO_2. For 2,5-HD treatment, fibroblasts were plated at the density of $1.2 \times 10^4/cm^2$ on uncoated 35 mm petri dishes; the day after, the cells were incubated for 24 h with different concentrations of 2,5-HD (Sigma-Aldrich), and then analysed. For the cell viability assay, the fibroblasts were grown with normal medium, which was changed just before the experiments with fresh medium containing a lower fetal bovine serum concentration (7.5% instead of 15%) and without β-mercaptoethanol, since both could interfere with MTT test.

2.3. 2,5-Hexanedione treatments on cells

Five-day NGF-differentiated PC12 cells were incubated for 24, 48 or 72 h with the following concentrations of 2,5-HD: 0.2 mM, 2 mM and 20 mM. Human fibroblasts were exposed to the same concentrations of 2,5-HD for 24 h. The 2,5-HD was diluted in the fresh appropriate culture medium and filtered. To start the treatment, the medium was changed with the one containing 2,5-HD and the cells were incubated in standard conditions. Once the incubations had finished, the living cells were observed by phase contrast microscopy and random images were captured for morphometric analyses. Immediately after, the cells were fixed with 4% paraformaldehyde (PFA) in phosphate-buffered saline (PBS, 20 mM Na-phosphate, 150 mM NaCl, pH 7.2) or cold methanol for immunofluorescence, lysed with cell lysis buffer for Western

blot analyses, or used for specific tests, such as cell viability or reactive oxygen species (ROS) production assays.

2.4. Morphometric analysis

The cell morphology of living cells at the end of treatment was evaluated by phase contrast microscopy. Five random images per well were captured at 20× magnification from at least 4 different wells per condition using Axiovert S100 microscope (Zeiss, Oberkochen, Germany) equipped with AxiocamHR (Zeiss) and then analysed using Axiovision Release 4.8 software (Zeiss). At least 400 differentiated cells per condition were considered for PC12 cells, while about 80 cells per condition and at least 20 per individual were analysed for human fibroblasts. For PC12, three principal features of neuritogenesis were considered: the percentage of differentiated cells, the length of the longest neurite for each differentiated cell and the percentage of differentiated cells presenting varicosities on their longest neurite. A cell was considered to have differentiated when its longest neurite was at least twice as long as its cell body diameter [44]. Regarding human fibroblasts, the maximum and the minimum axes, their ratio and the cell area were measured.

2.5. Cell viability assay

Cells, previously treated with different concentrations of 2,5-HD, were incubated with a freshly prepared solution (0.5 mg/ml) of 3-(4,5-dimethylthiazol-2-yl)-2,5-diphenyltetrazolium bromide salt (MTT, Sigma-Aldrich). After 3 h of incubation at 37 °C, a solution of 0.1 M HCl in isopropanol was added to each well in equal volume. The intensity of purple colour of formazan crystals in each well was measured through a plate-reader spectrophotometer (Infinite 200Pro, Tecan, Mannedorf, Switzerland) at wavelength of 570 nm.

2.6. DCFDA assay

ROS production was detected using 2′,7′-dichlorofluorescin diacetate (DCFDA) Cellular ROS Detection Assay Kit (Abcam, Cambridge, UK) according to manufacturer's instructions. Briefly, NGF-differentiated PC12 cells were grown in a black multiwell and after 5 days of differentiation were incubated for 45 min with 25 μM DCFDA at 37 °C. After incubation, the cells were washed once with the kit buffer and then treated with 2,5-HD for 24 h. Tert-butyl hydrogen peroxide (TBHP, 50 μM for 3 h) that mimics ROS activity was used as positive control. The fluorescence intensity was finally measured through a plate-reader spectrophotometer (Infinite 200Pro, Tecan) using the excitation/emission wavelength 485 nm/535 nm.

2.7. Analysis of mitochondrial network morphology

For staining the active mitochondria MitoTracker Red CMX-Ros (M7512, Thermo Fisher Scientific) was used according to manufacturer's protocol. Briefly, NGF-differentiated PC12 cells treated with 2,5-HD for 24 h were incubated for 40 min with 500 nM MitoTracker Red CMX-Ros and fixed for 10 min with 4% PFA in PBS. The samples were also counterstained with DAPI to visualize the nuclei and mounted in Mowiol (Calbiochem, San Diego, CA)-DABCO (Sigma-Aldrich). The mitochondrial network morphology was investigated only in the soma of PC12 cells by confocal microscopy performed on a Leica TCS SP5 confocal laser scanning microscope (Leica Microsystems, Heidelberg, Germany). The images were acquired using LAS AF software (Leica) with an HCX PL APO 63X/1.4NA oil immersion objective and 405 nm and 561 nm laser lines. By means of ImageJ software (NIH, Bethesda, USA), each isolated soma was cropped out from the raw images. The resulting regions of interest (ROI) were then binarized after the application of an intensity-based threshold. The outlines of the network were then selected and mitochondrial area and perimeter were measured. The form factor was calculated (defined as $[P_m{}^2]/[4\pi A_m]$), where P_m is the length of the mitochondrial perimeter and A_m is the area of the mitochondria [45]. The form factor allows quantifying the degree of branching of the mitochondrial network. At least 15 randomly distributed fields were acquired for each experimental condition and at least 50 cells for condition were analysed.

2.8. Western blot analysis

Whole cell extracts, Triton X-100 (Sigma-Aldrich)-soluble and -insoluble fractions of PC12 cells and human fibroblasts were prepared and analysed as previously reported [46]. After SDS-PAGE, proteins were transferred onto polyvinylidene difluoride membrane (Immobilon-FL IPLL00010; Millipore, Darmstadt, Germany) and incubated overnight at 4 °C with the following primary antibodies: anti-actin mouse IgM (N350, Amersham, Little Chalfont, UK) 1:4000; anti- neurofilament light protein (NF-L) rabbit IgG (AB-10685, Immunological Sciences, Rome, Italy) 1:40000, anti- neurofilament medium protein (NF-M) mouse IgG (MAB-10338, Immunological Sciences) 1:40000, anti-α-tubulin mouse IgG (clone B-5-1-2, T6074, Sigma-Aldrich) 1:1000; anti-detyrosinated tubulin rabbit IgG (ab 48389, Abcam) 1:1000; anti-tyrosinated tubulin mouse IgG (clone TUB-1A2, Sigma-Aldrich) 1:1000; anti-acetylated tubulin mouse IgG (clone 6-11B-1, T7451, Sigma-Aldrich) 1:2000; anti-dynamin-related protein 1 rabbit IgG (clone D6C7, #8570, Cell Signaling, Danvers, MA, USA) 1:1000; anti-mitofusin-2 rabbit IgG (clone D2D10, #9482, Cell Signaling) 1:1000; anti-voltage-dependent anion channel 1 (VDAC) rabbit IgG (ab15895, Abcam) 1:500; anti-microtubule-associated protein 1 light chain 3 (LC3) rabbit IgG (L8918, Sigma) 1:2000; anti-HRP-glyceraldehyde 3-phosphate dehydrogenase (GAPDH) mouse IgG2b (mAbcam 9484, Abcam) 1:3000. Membranes were washed for 30 min with 3 changes and incubated for 1 h at room temperature with horseradish peroxidase (HRP) goat anti-mouse IgG (31430, Pierce) 1:20000, HRP goat anti-rabbit IgG (31460, Pierce) 1:40000 or HRP goat anti-mouse IgM (ab5930, Abcam) 1:5000. For LC3 we used as secondary antibodies Alexa Fluor 488 goat anti-rabbit (ab150077, Abcam) 1:4000. The reaction was developed using a chemiluminescent immunoassay (Super-Signal West Pico Chemiluminescent, Pierce). To ensure equal protein loading for the whole protein lysates (not for Triton-soluble/insoluble fractions), protein samples were assayed by densitometry of Coomassie blue-stained PVDF membranes and adjusted for blotting. Immunoblots were scanned with Epson WP-4525 colour image scanner (Seiko Epson Corporation, Suwa, Japan) and their quantitation was performed by ImageJ software. For LC3 and GAPDH acquisition and quantification were performed by Chemidoc and Image Lab software (Bio-Rad, Hercules, CA, USA).

2.9. Immunofluorescence and labeling on PC12 cells

Cells were fixed with methanol at −20 °C or 4% PFA for 10 min and incubated with the following primary antibodies, previously used for immunoblotting, and probes: Atto 565 Phalloidin (94072, Sigma-Aldrich) 1:100; NF-L rabbit IgG 1:1000; α-tubulin mouse IgG 1:500; detyrosinated tubulin rabbit IgG 1:100; tyrosinated tubulin mouse IgG 1:100; acetylated tubulin mouse IgG 1:100; and 4′,6-Diamidino-2-phenylindole dihydrochloride DAPI (D-8417, Sigma-Aldrich) 1:40000. As secondary antibodies we used: Alexa Fluor 568 goat anti-mouse (A11004, Thermo Fisher Scientific) 1:1000; Alexa Fluor 488 goat anti-rabbit (ab150077, Abcam) 1:1000. The coverslips were mounted in Mowiol-DABCO and samples were examined with the Axiovert 200 M microscope (Zeiss). Furthermore, the cells showing a perinuclear accumulation of detyrosinated MTs were counted and the percentage respect to the total number of differentiated cells was calculated for each experimental condition. At least 15 randomly distributed fields were acquired for each experimental condition and at least 770 cells for condition were analysed.

2.10. Tubulin assembly in vitro

Tubulin was purified from fresh bovine brain conserved in ice-cold PBS. Pure tubulin was obtained by two cycles of polymerization-depolymerization in a high-molarity buffer [47] resuspended in BRB80 (80 mM K-Pipes pH 6.9, 2 mM EGTA, 1 mM $MgCl_2$; all from Sigma-Aldrich), snap-frozen in liquid nitrogen, and stored in small aliquots at −80 °C. The kinetics of tubulin polymerization was studied using a standard protocol [48] in the absence or presence of different concentration of 2,5-HD. Reactions were followed turbidimetrically at 350 nm for 90 min at 37 °C in a multimode plate reader (Infinite 200Pro, Tecan) equipped with a temperature controller. Pure bovine brain tubulin was diluted in a previously degassed assembly buffer (80 mM K-Pipes, pH 6.9, 2 mM EGTA, 1 mM $MgCl_2$, 10% glycerol, and 1 mM GTP) to the working concentration of 30 μM and kept on ice; the reaction was started by heating up the solution to 37 °C. Polymerization time-course was dissected in order to calculate the kinetic parameters describing the different phases of the process as previously reported [48]. The number of successive steps in the nucleation (P) was determined by plotting $\log(A(t)/A\infty)$ against $\log(t)$. The maximal velocity of polymerization (V_i) was calculated as the variation of mass versus time ($\delta A/\delta t$) at the very initial elongation phase, whereas total extent of MT assembly was deduced from the total absorbance variation (ΔA) achieved as the steady-state was established.

2.11. Electron microscopy

Negative staining of pure tubulin was prepared by leaving a drop of assembled MTs, previously fixed with 1% (v/v) glutaraldehyde, on Formvar Carbon Film-coated 200 square mesh Nickel grids (FCF200-Ni-50, Electron Microscopy Sciences, Hatfield, PA, USA) for 30 min at 25 °C. The grids were first washed three times with 5 mM EGTA, then dipped rapidly twice in 1% uranyl acetate and let dry on filter paper at room temperature. The transmission electron microscopy images were obtained with a Zeiss LEO 912AB Energy Filtering TEM operating at 80 kV. Digital images were acquired using a CCD-BM/1K camera operating with iTEM software (Olympus).

2.12. Animals

All mice were kept in pathogen-free conditions and all procedures complied with the Italian law D.lgs 116/92 and were approved by the University of Milan Animal Welfare Body and by Italian Ministry of Health (protocol number 6/2012). Wild-type C57BL mice were purchased from Charles River (Calco, Italy) and used for all experiments. Mice were kept under environmentally controlled conditions (ambient temperature 22 °C; humidity 40%) on a 12-hour light/dark cycle with food and water ad libitum.

2.13. 2,5-Hexanedione treatments on animals

Fifteen-month old mice were treated with intraperitoneal injections of 2,5-HD 8 mmol/kg for 19 consecutive days, as previously reported [30]. Control mice were injected with saline. Twenty-four hours after last injection of 2,5-HD, mice were sacrificed in order to fix and process the brains for immunohistochemical and immunofluorescence analyses. Mice were deeply anesthetized and transcardially perfused with 4% PFA in 0.1 M phosphate buffer pH 7.4 as previously described [49]. Brains were removed, postfixed 3 h in 4% PFA and then cut with a vibratome (VT1000S; Leica) in both coronal and sagittal sections (50 μm thick) to be used for immunohistochemical and immunofluorescence stainings, respectively. Part of the sections was cryoprotected for long-term conservation at −20 °C.

2.14. Immunohistochemistry of tyrosine hydroxylase with diaminobenzidine

Free-floating coronal sections (50 μm thick) were selected at different rostro-caudal levels of *Substantia nigra pars compacta* or *Corpus striatum* and were immunolabeled with an antibody against tyrosine hydroxylase (TH) according to a standard immunoperoxidase protocol. Briefly, the selected sections were incubated overnight at 4 °C with the primary antibody anti-TH rabbit IgG (1:200; Millipore) and then incubated with biotin-labeled goat anti-rabbit IgG antibody (1:200; Vector Laboratories, Inc., Burlingame, CA, USA) for 75 min. Immunoreactivities were visualized by avidin-biotin HRP complex (ABC Elite; Vector Laboratories) using the chromogen 3,3′-diaminobenzidine tetra-hydrochloride (DAB, Roth, Karlsruhe, Germany) for detection.

2.15. Stereological counts of tyrosine hydroxylase-positive neurons in Substantia nigra pars compacta

To estimate the total number of TH-positive cells in the entire *Substantia nigra pars compacta*, we performed stereological cell countings using the optical fractionator method on workstation with the stereological software StereoInvestigator7 (MicroBright-Field Inc., Colchester, Vermont, USA) connected to a Leica DMLB microscope equipped with a motorized stage and coupled to a Retiga 2000R colour uncooled camera. The stereological analysis was performed on 7 coronal sections of 50 μm per animal, sampled every 150 μm, in which the *Substantia nigra pars compacta* was identified and outlined at 4× magnification, while the counts of TH-positive cells were conducted at 40× magnification. For stereological counting, we used a grid of dissectors (counting frame 50 × 50 μm; grid size 100 × 100 μm) and the final analysed section thickness was about 26 μm in the *Z*-axis. The TH-positive cells were counted only as they came into focus within the counting frame area and also if touching or crossing the inclusion lines. The estimated total number of TH-positive cells in the *Substantia nigra pars compacta* was computed from the formula: $N = \Sigma(n) \times 1/SSF \times 1/ASF \times 1/TSF$, where n is the total number of TH-positive cells counted on each dissector; SSF (section sampling fraction) is the number of regularly spaced sections used for counts divided by the total number of sections across the *Substantia nigra pars compacta*; ASF (area sampling fraction) is the total area of all dissectors divided by the total area of all the regions drawn on the sections ($2500\ \mu m^2 \times$ dissector number/total area of all regions to be counted); and TSF (thickness sampling fraction) is the dissector thickness (26 μm) divided by the section thickness (50 μm). The precision of the estimate of total number of TH-positive cells in each subject was evaluated as the coefficient of error and the sampling was considered optimal when this was < 0.05.

2.16. Densitometric analysis of tyrosine hydroxylase-positive axonal terminals in Corpus striatum

For the densitometric analysis, 2 coronal sections per animal were collected from the *Corpus striatum* between +1.08 mm and +0.14 mm according to bregma in the mouse brain atlas [50]. Densitometric analysis of TH-positive axonal terminals in *Corpus striatum* was performed using ImageJ software measuring the optical density (O.D.). The selected coronal sections were acquired with a Leica DMLB microscope coupled to a Retiga 2000R colour uncooled camera using a 2.5× objective. Once done the O.D. calibration in ImageJ to convert the grey scale values in O.D. values, the following ROIs were identified and outlined for each section: the total striatum, the dorsal striatum and the dorso-lateral striatum. The mean O.D. values were measured for all the regions. The background value for each section was measured in the *Corpus callosum* and was then subtracted from the mean values measured in all the ROIs of the *Corpus striatum*. Subsequently, the mean value of two sections per animal was calculated before the data were

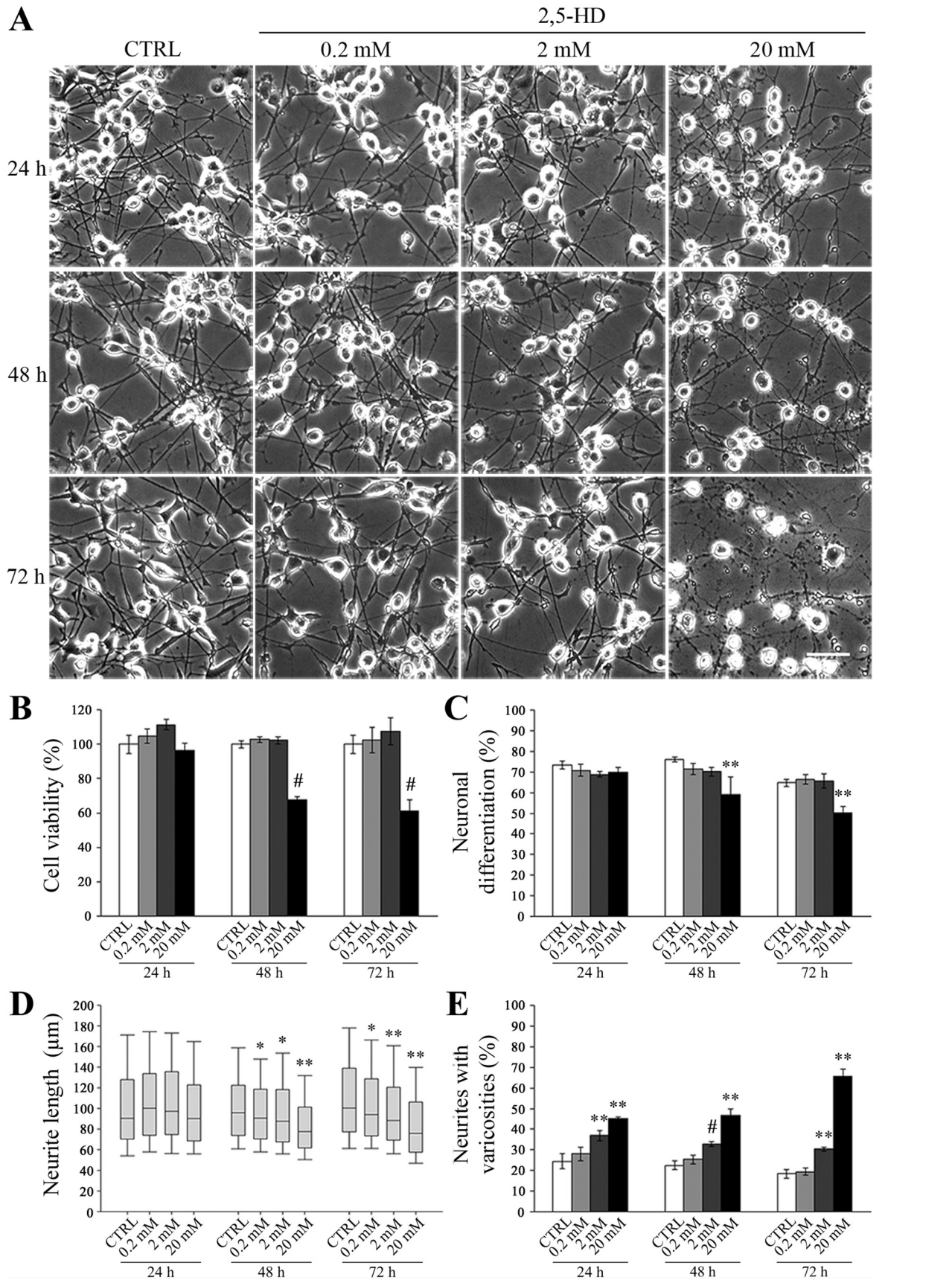

(caption on next page)

Fig. 1. 2,5-Hexanedione induces morphological changes in NGF-differentiated PC12 cells.
(A) Representative phase contrast images of 5-day NGF-differentiated PC12 cells treated with different concentrations of 2,5-HD. Scale bar: 50 μm. (B) Cell viability, evaluated by MTT assay, was affected only at 20 mM after 48 and 72 h of exposure. $^{\#}p < 0.01$ vs control (CTRL) according to one-way ANOVA, Dunnett post hoc test. (C–E) Morphometric analyses revealed significant morphological alterations induced by 2,5-HD in a dose-dependent manner. Three principal features of neuritogenesis were considered: the percentage of differentiated cells (histogram, C), the length of the longest neurite for each differentiated cell (box plot, D) and the percentage of differentiated cells presenting varicosities on their longest neurite (histogram, E). 2,5-HD treatment induced the shortening of neurites' length with consequent reduction in differentiated state of the cells and induced the formation of small axonal swelling. All values are expressed as mean ± SEM. For the percentage of neuronal differentiation (C) and neurites with varicosities (E) $^{\#}p < 0.01$ and $^{**}p < 0.001$ vs CTRL according to χ^2 test. For the neurite length (D) $^{*}p < 0.05$ and $^{**}p < 0.001$ vs CTRL according to one-way ANOVA, Dunnett post hoc test.

processed statistically.

2.17. Immunofluorescent staining, confocal microscopy and image analysis

For the immunofluorescence analysis, 2 sagittal sections per animal, containing the entire nigrostriatal pathway, were collected. Selected free-floating sections were incubated overnight at 4 °C with the following primary antibodies: anti-tyrosinated tubulin rat IgG (clone YL 1/2; Abcam) 1:100; anti-detyrosinated tubulin rabbit IgG 1:500, and anti-acetylated tubulin mouse IgG 1:500. To identify the dopaminergic neuronal structures (soma, fibers and terminals), each section was concurrently stained with anti-TH antibody made in mice (clone LCN1; Millipore) 1:200 or rabbits 1:200 as appropriate. After several rinses in PBS, the sections were incubated in the following secondary antibodies: Alexa Fluor 488 goat anti-mouse IgG, Alexa Fluor 488 goat anti-rabbit IgG, Alexa Fluor 568 donkey anti-mouse IgG, Alexa Fluor 568 donkey anti-rabbit IgG and Alexa Fluor 568 donkey anti-rat IgG (Thermo Fisher Scientific). Just the section in Fig. 7A, showing an overview of the nigrostriatal pathway, was also counterstained with DAPI (1:4000) for 15 min before the mounting step. Finally, the samples were mounted in PBS-glycerol. Confocal microscopy was performed on these samples with a Leica TCS SP5 confocal laser scanning based on a Leica DMI 6000B inverted microscope. The images were acquired with a HCX PL APO 40X/1.25NA oil immersion objective using 488 nm and 561 nm laser lines. The software used for all acquisitions was Leica LAS AF. Once the parameters of acquisition for control conditions had been defined, they were kept constant for all the samples. Images were acquired in three different brain regions: *Substantia nigra pars compacta*, the nigrostriatal fibers' region and the dorsal part of *Corpus striatum*. Quantification of the mean fluorescence intensity inside dopaminergic neurons was performed using ImageJ software. For the region of *Substantia nigra pars compacta*, only somas in which the nucleus was clearly evident have been selected for the analysis and the perimeter was manually drawn excluding the area occupied by the nucleus from each cell area. The ROIs were drawn using the TH channel and subsequently applied on the channel of the selected α-tubulin PTM. Similarly, for nigrostriatal fibers and *Corpus striatum* regions, a mask was created using an appropriate threshold for every image on the TH channel and then applied onto the channel of the selected α-tubulin PTM.

2.18. Statistical analyses

Data from two experimental groups were analysed by paired/unpaired Student's *t*-test and the normal distribution of experimental data was previously assessed with the Kolmogorov-Smirnov test, using the Prism 8 (GraphPad Software, Inc.) software. In the case of more than two experimental groups, statistical analyses were performed by one-way analysis of variance (ANOVA) followed by Tukey HSD, Fisher LSD or Dunnett 2-sided test as post hoc multiple comparison test using STATISTICA7 software (StatSoft Inc., Tulsa, OK). When the distribution was not normal, data were analysed using the non-parametric Mann-Whitney U or Kruskal-Wallis test for the comparison between two or more groups, respectively. Finally, χ^2 test was used to analyse qualitative variables, as appropriate. Data are expressed as means ± SEM. All experiments were repeated at least three times. $p < 0.05$ was considered statistically significant.

3. Results

3.1. 2,5-Hexanedione induces morphological changes in NGF-differentiated PC12 cells

We started our investigation about the effects of 2,5-HD on NGF-differentiated PC12 cell line, as it is a well-characterized model of cultured dopaminergic neurons [51], which are the neurons that are selectively lost in PD. In order to set up the PD toxin assays, the optimisation of the exposure time was carried out by treating 5-day NGF-differentiated PC12 cells with different concentrations of 2,5-HD (0.2, 2, 20 mM) for 24, 48, and 72 h (Fig. 1). Firstly, the toxin effect on cell viability was examined by MTT test, showing that cell survival was significantly reduced only at the highest concentration of 2,5-HD after 48 and 72 h, but not after 24 h (Fig. 1B). In parallel, the observation of living cells by phase contrast technique revealed some morphological alterations of the treated cells (Fig. 1A). In order to quantify these changes, morphometric analyses were performed to evaluate the percentage of differentiated cells (Fig. 1C), the neurite length of differentiated cells (Fig. 1D) and the percentage of neurites with axonal swellings, called varicosities (Fig. 1E). According to these analyses, 2,5-HD induced the shortening of neurite length with consequent reduction in differentiated phenotype after 48 and 72 h (Fig. 1C–D). Moreover, 2,5-HD was also able to induce the formation of varicosities along neurites already at 2 mM after 24 h of treatment (Fig. 1E). Based on these observations, we conclude that 2,5-HD affects cell morphology in NGF-differentiated PC12 cells leading to major alterations over time. Taking into account that cell viability was not yet affected within the first 24 h of toxin exposure, this administration scheme was applied as a good experimental paradigm to investigate the early events of neurodegeneration in subsequent experiments.

3.2. Mitochondria are altered by high doses of 2,5-hexanedione

Since the most common PD toxins, such as MPP^+ or rotenone, are potent inhibitors of complex I of the electron transport chain, mitochondrial dysfunction has been considered one of the principal culprits of neuronal death in PD, together with oxidative stress and protein degradation inefficiency, for a long time [52]. To verify this hypothesis, we looked at the impact of 24 hour-treatment with 2,5-HD on oxidative stress and mitochondrial dynamics (Fig. 2) in the same conditions in which we had already observed alterations in cell morphology. In order to quantify ROS production, the DCFDA assay was performed, revealing that a significant increase in ROS was induced only by the highest concentration (20 mM) (Fig. 2A). Moreover, the levels of dynamin-related protein 1 and mitofusin 2, two crucial proteins regulating mitochondrial fission and fusion respectively [53], were investigated by Western blot analysis. Both protein levels were decreased only at the highest dose of toxin (Fig. 2B–C). Finally, in order to analyse the mitochondrial network morphology, we evaluated the degree of mitochondrial branching. Notably, the network was altered following incubation with 20 mM 2,5-HD (Fig. 2D–E) and the significant decreased of branching was revealed by the analysis of the form factor value (Fig. 2F). Interestingly, 2,5-HD strongly affects neuronal morphology already at 2 mM, whereas mitochondrial defects are detectable only at 20 mM, allowing us to speculate that they could be a possible

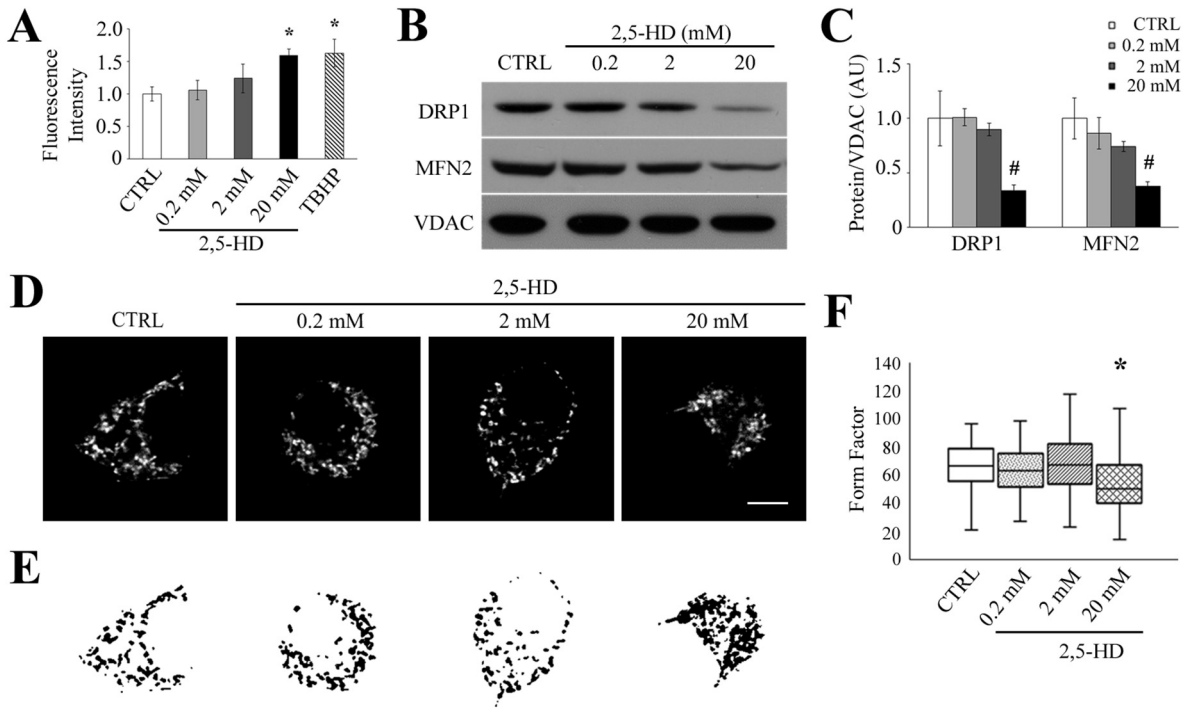

Fig. 2. Mitochondria are altered by high doses of 2,5-hexanedione.
(A) Reactive oxygen species (ROS) production was measured using DCFDA Cellular ROS Detection assay on 5-day NGF-differentiated PC12 cells treated for 24 h with different concentrations of 2,5-HD. Tert-butyl hydrogen peroxide (TBHP, 50 μM for 3 h), which mimics ROS activity, was used as positive control. The data are expressed as fold change with respect to control (mean ± SEM). *$p < 0.05$ vs control according to one-way ANOVA, Fisher LSD post hoc test. (B) Immunoblot and (C) densitometric analyses of dynamin-related protein 1 (DRP1) and mitofusin-2 (MFN2) were performed in whole cell extracts from 5-day NGF-differentiated PC12 cells treated for 24 h with different concentrations of 2,5-HD. For the quantitation, values of each mitochondrial protein were normalized on the level of mitochondrial porin (VDAC) of the relative sample. All values are expressed as mean ± SEM. The data are expressed as fold change with respect to control (mean ± SEM). $^{\#}p < 0.01$ vs control according to one-way ANOVA, Fisher LSD post hoc test. (D) Representative images of the mitochondrial network labeled with MitoTracker Red CMX-Ros in soma of NGF-differentiated PC12 cells after 24-hour treatment with 2,5-HD. Scale bar: 5 μm. (E) Corresponding binarized masks used to estimate the degree of mitochondrial branching (form factor). (F) Box plot displaying the form factor values obtained for the analysis of mitochondrial network morphology. The form factor value was significantly decreased only at 20 mM respect to control. *$p < 0.05$ vs CTRL according to Kruskal-Wallis test, at least 50 cells for each group were analysed.

consequence of the impairment of other frailer systems.

3.3. 2,5-Hexanedione impacts on all the components of the cytoskeleton in NGF-differentiated PC12 cells

In accordance with previous works suggesting that 2,5-HD affects cytoskeletal components [28], we hypothesized that the observed morphological changes probably derived from dysfunction of the overall cytoskeleton. Thus, the characterization of all its components (actin filaments, NFs and MTs) after 24 h of toxin treatment was carried out with both biochemical and immunocytochemical approaches (Fig. 3). The Western blot and its densitometric analysis (Fig. 3A–B) revealed a significant decrease in the levels of both NF-L and NF-M at the highest concentration, while the overall content of α-tubulin and actin remained unchanged. In parallel, immunofluorescence stainings were performed to investigate distribution and organization of the three cytoskeletal filaments in detail (Fig. 3C). Actin showed a particular organization in bundle-like structures at 2 mM of 2,5-HD. Interestingly, this kind of rearrangement of microfilaments into ruffles has been described also in epithelial cells [54]. As expected and already described in the literature in other neuron-like cellular models [55,56], NF-L (Fig. 3C), as well as NF-M (data not shown), collapsed into varicosities and in the perinuclear zone in a dose-dependent manner. The α-tubulin staining, instead, highlighted marked dose-dependent fragmentation of the MT cytoskeleton along neurites and also an unusual perinuclear accumulation (Fig. 3C). These data revealed that 2,5-HD impacts all the cytoskeletal components in NGF-differentiated PC12 cells and, to the best of our knowledge, these results show for the first time the loss of integrity of MTs following 2,5-HD treatment, which could likely lead to the impairment of axonal transport and, consequently, to the accumulation of NFs since they are transported along axons in a MT-dependent manner [57].

3.4. 2,5-Hexanedione causes the imbalance of α-tubulin PTMs, changing microtubule distribution and stability in NGF-differentiated PC12 cells

The above reported results strongly suggest that the MT cytoskeleton is a relevant target of 2,5-HD and plays a key role in PD-related neurodegenerative processes. To verify this hypothesis we carried out a more in-depth investigation of MTs through the analysis of different α-tubulin PTMs (Fig. 4) that specifically correlate with subsets of MTs characterized by different stability [58]. Surprisingly, unlike the overall amount of α-tubulin, which was not significantly changed (Fig. 3A–B), the biochemical approach showed significant differences in PTM levels at 20 mM of 2,5-HD (Fig. 4A–B). In fact, the Western blot analysis revealed a significant increase in the level of detyrosinated tubulin, marker of stable MTs, and a concurrent decrease in the level of tyrosinated tubulin, associated to dynamic MTs (Fig. 4A–B). The alteration in stable MTs was also highlighted by immunofluorescence staining, which revealed perinuclear accumulation of both detyrosinated and acetylated tubulin, as well as their fragmentation, at the highest dose of 2,5-HD (Fig. 4C). We calculated the percentage of differentiated cells that exhibits the perinuclear accumulation of detyrosinated tubulin and we found a significant increase already at 0.2 mM 2,5-HD (Fig. 4D).

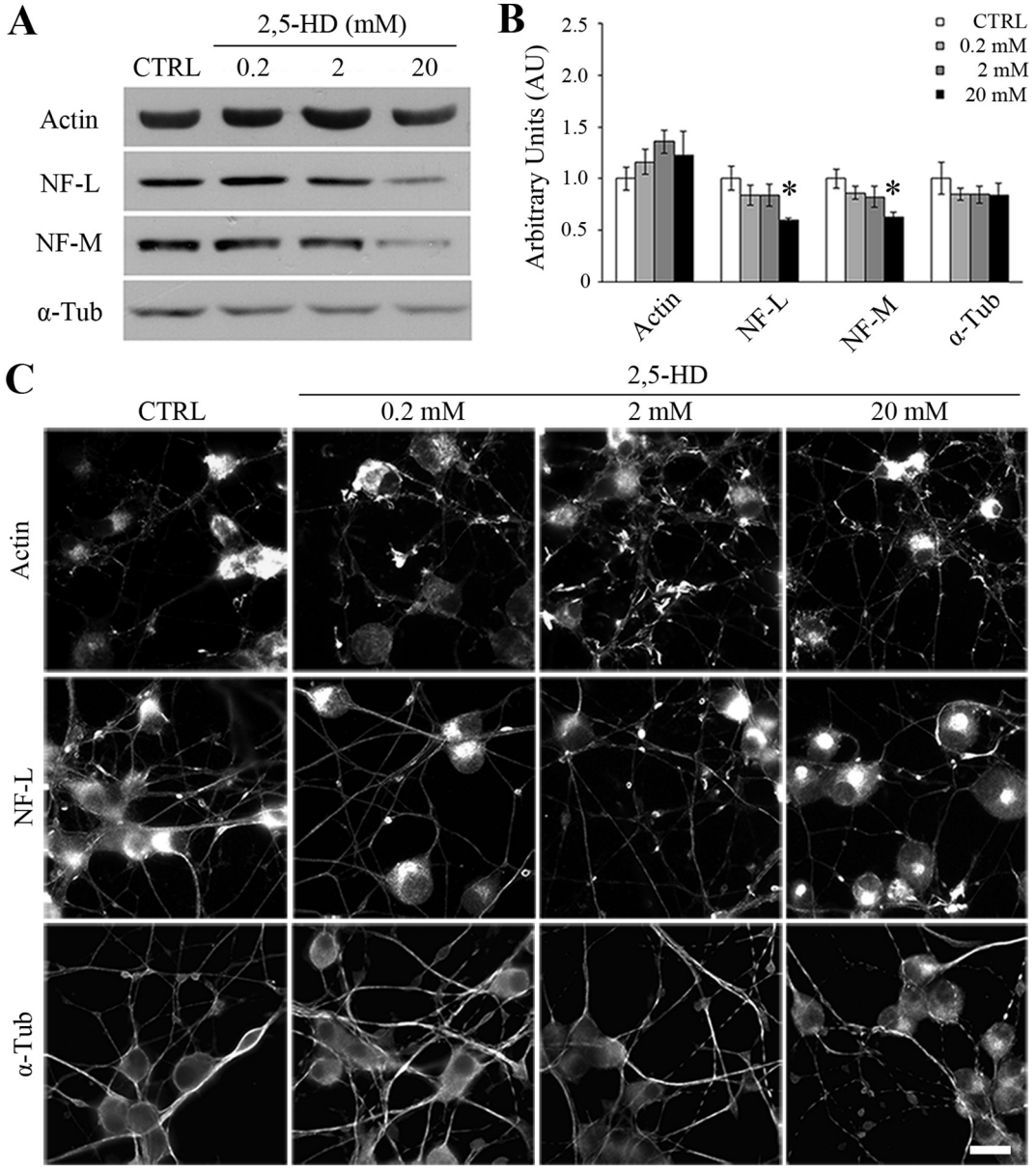

Fig. 3. 2,5-Hexanedione impacts on all the components of the cytoskeleton in NGF-differentiated PC12 cells.
(A) Immunoblot and (B) densitometric analyses of actin (Actin), neurofilament light protein (NF-L), neurofilament medium protein (NF-M) and α-tubulin (α-Tub) were performed in whole cell extracts from 5-day NGF-differentiated PC12 cells treated for 24 h with different concentrations of 2,5-HD. For the quantitation, values of each protein were normalized on the total amount of proteins loaded per lane, through the Coomassie blue staining. The data are expressed as fold change with respect to control (mean ± SEM). *$p < 0.05$ vs control (CTRL) according to one-way ANOVA, Fisher LSD post hoc test. (C) NGF-differentiated PC12 cells were stained with Atto565-conjugated phalloidin or with primary anti-NF-L and anti-α-tubulin antibodies to reveal the organization of actin fibers (Actin, top), neurofilaments (NF-L, middle) and microtubules (α-Tub, bottom), respectively, and acquired with a widefield fluorescence microscope. Scale bar: 20 μm.

Furthermore, in order to verify whether the observed intracellular accumulation was correlated with the activation of the autophagic pathway, we checked for the levels of LC3-I and -II, well known marker of autophagy. We observed no significant changes induced by 2,5-HD in LC3-I (Fig. S1A–B), whereas the LC3-II protein levels were too low to be quantified (Fig. S1C). Indeed, we did not detect any conversion of LC3-I to LC3-II which is a reliable indicator of autophagic activity (Fig. S1). The abnormal organization of stable MTs may be evidence of greater changes in the MT system, which can cause the impairment of axonal transport, with consequent accumulation of proteins and organelles [39], such as the accumulation of NFs in the cell body we showed in Fig. 3C. These results also offer an explanation for the neurite retraction and the reduction of neuronal phenotype caused by 2,5-HD exposure longer than 24 h in NGF-differentiated PC12 cells (Fig. 1C–D).

To further investigate the effect of the toxin on MT stability, we studied the ratio between the free and polymerized form of *in cell* α-tubulin and the *in vitro* kinetics of tubulin assembly in the presence of 2,5-HD (Fig. 5). In order to study the state of *in cell* tubulin assembly (Fig. 5A–B), we analysed the tubulin fractions composed by free dimers with respect to polymerized MTs. The highest toxin concentration of 2,5-HD caused the shift of tyrosinated tubulin towards the dimer pool, suggesting depolymerization of MT system and consequent decrease in MT stability. Moving to the *in vitro* assay, we analysed the assembly kinetics of pure tubulin in the presence of increasing concentrations of 2,5-HD (Fig. 5C) and calculated the following parameters (Table 1): *P* value for nucleation phase, the initial velocity of polymerization (V_i) and the final absorbance at 350 nm (ΔA). No significant changes in the assembly curves and in the parameters defining the different phases

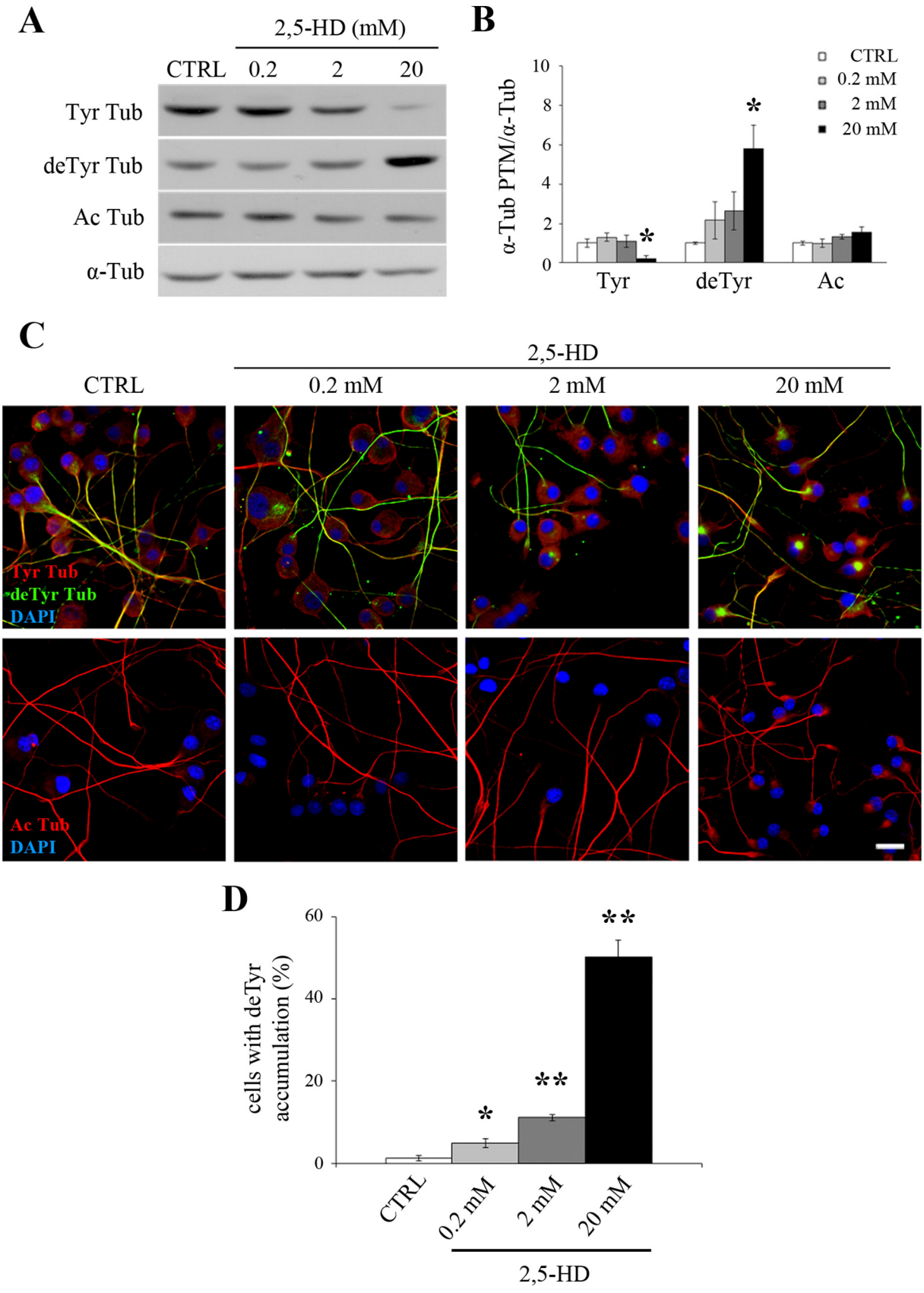

(caption on next page)

Fig. 4. 2,5-Hexanedione causes the imbalance of α-tubulin PTMs in NGF-differentiated PC12 cells.
(A) Immunoblot and (B) densitometric analyses of post-translational modifications (PTMs) of α-tubulin (α-Tub): tyrosinated tubulin (Tyr Tub), detyrosinated tubulin (deTyr Tub) and acetylated tubulin (Ac Tub). The analyses were performed on whole cell extracts from 5-day NGF-differentiated PC12 cells treated for 24 h with different concentrations of 2,5-HD. For the quantitation, the levels of α-tubulin PTMs were normalized firstly on the total amount of proteins loaded per lane, through the Coomassie blue staining, and then on the total level of α-tubulin in the respective sample. The data are expressed as fold change with respect to control (mean ± SEM). *p < 0.05 vs control (CTRL) according to one-way ANOVA, Fisher LSD post hoc test. (C) 2,5-HD alters the distribution of stable microtubules, the ones characterized by the presence of detyrosinated and acetylated α-tubulin. NGF-differentiated PC12 cells were stained for tyrosinated (Tyr Tub, red), detyrosinated (deTyr Tub, green) and acetylated tubulin (Ac Tub, red) to investigate microtubule organization and acquired with a widefield fluorescence microscope. All cells were also concurrently stained with DAPI (blue) to visualize the nuclei. Scale bar: 20 μm. (D) Percentage of NGF-differentiated PC12 cells presenting accumulation of detyrosinated microtubules in perinuclear zone respect to the total number of differentiated cells. 2,5-HD significantly increased the percentage of cells with the accumulation of stable microtubules (deTyr Tub) at each dose of treatment. All values are expressed as mean ± SEM. *p < 0.05 and **p < 0.001 vs CTRL according to χ^2 test, at least 770 cells for each group were analysed. (For interpretation of the references to colour in this figure legend, the reader is referred to the web version of this article.)

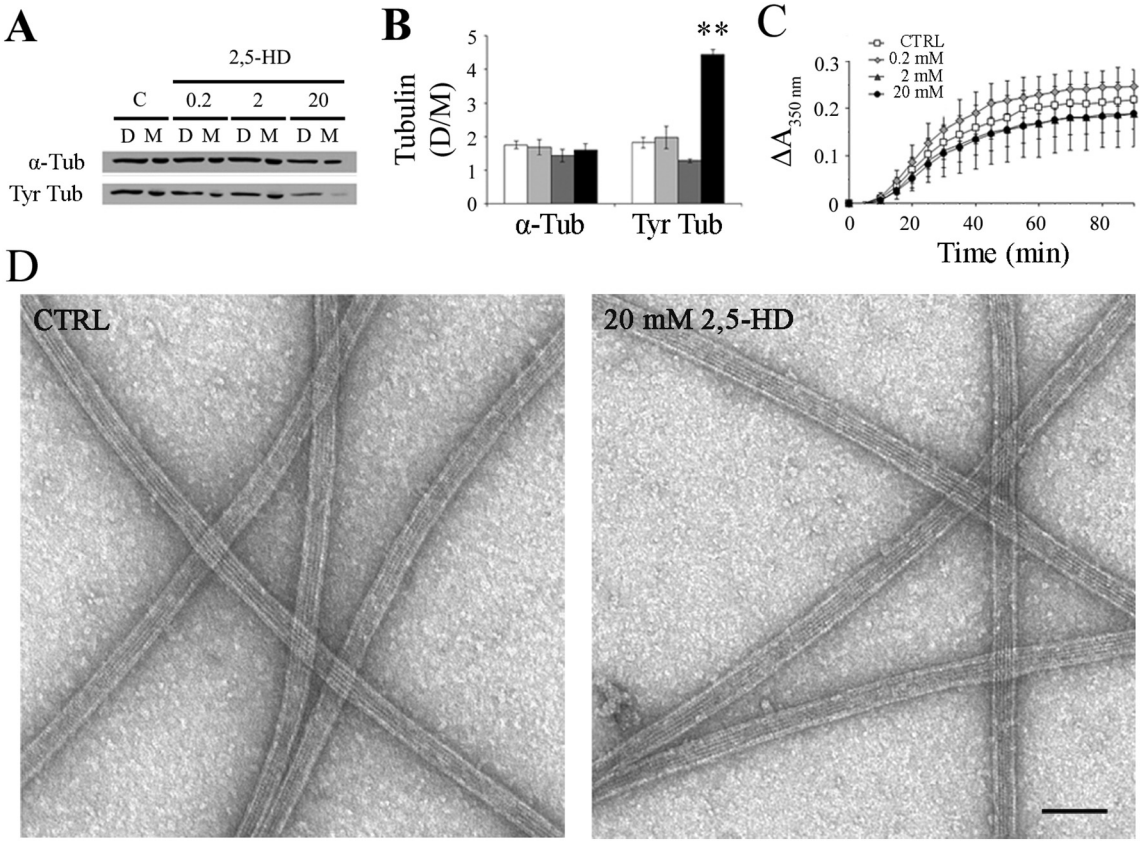

Fig. 5. 2,5-Hexanedione alters microtubule stability in NGF-differentiated PC12 cells, but does not affect tubulin polymerization kinetics and microtubule ultrastructure *in vitro*.
(A–B) Triton-X100-soluble (representing the α-tubulin dimer pool, D) and -insoluble fraction (α-tubulin incorporated into microtubules, M) of α-tubulin (α-tub) and its tyrosinated form (Tyr Tub) in NGF-differentiated PC12 cells were analysed by (A) immunoblot and (B) densitometric analyses, shown as ratio. 2,5-HD influenced the tubulin distribution between the two fractions. Interestingly, the ratio was shifted towards the free-tubulin fraction, at the highest dose of toxin, only for the tyrosinated form of tubulin. All values are expressed as mean ± SEM. **p < 0.001 vs control (CTRL) of each group according to one-way ANOVA, Tukey HSD post hoc test. (C) Representative kinetic curves of pure bovine brain tubulin (30 μM) polymerized in assembly buffer in the absence (CTRL) or presence of different concentrations of 2,5-HD. Reactions were followed turbidimetrically at 350 nm for 90 min at 37 °C. (D) Ultrastructure of microtubules assembled in absence or presence of 2,5-HD in the same conditions described above for the kinetic curves. The microtubules assembled *in vitro* were fixed with 0.5% glutaraldehyde prior to perform the negative staining with uranyl acetate. CTRL and 20 mM 2,5-HD treated tubulin are shown: the ultrastructure of microtubules is not affected by 2,5-HD in the tested conditions. Scale bar: 100 nm.

Table 1
Kinetic parameters of tubulin assembly in the presence of 2,5-hexanedione.

Kinetic parameters	CTRL	0.2 mM	2 mM	20 mM
P value	4.00 ± 0.25	4.22 ± 0.23	4.91 ± 0.45	4.77 ± 0.79
V_i	0.0067 ± 0.0017	0.0079 ± 0.0021	0.0057 ± 0.0037	0.0043 ± 0.0015
ΔA	0.221 ± 0.029	0.253 ± 0.036	0.196 ± 0.084	0.192 ± 0.035

The table reports the kinetic parameters calculated from the polymerization curves: the number of successive steps in the nucleation phase (*P* value), the maximal velocity of polymerization at the very initial elongation phase (V_i, ΔA/min) and the total extent of microtubule assembly as the total absorbance variation (ΔA). All values are expressed as mean ± SEM.

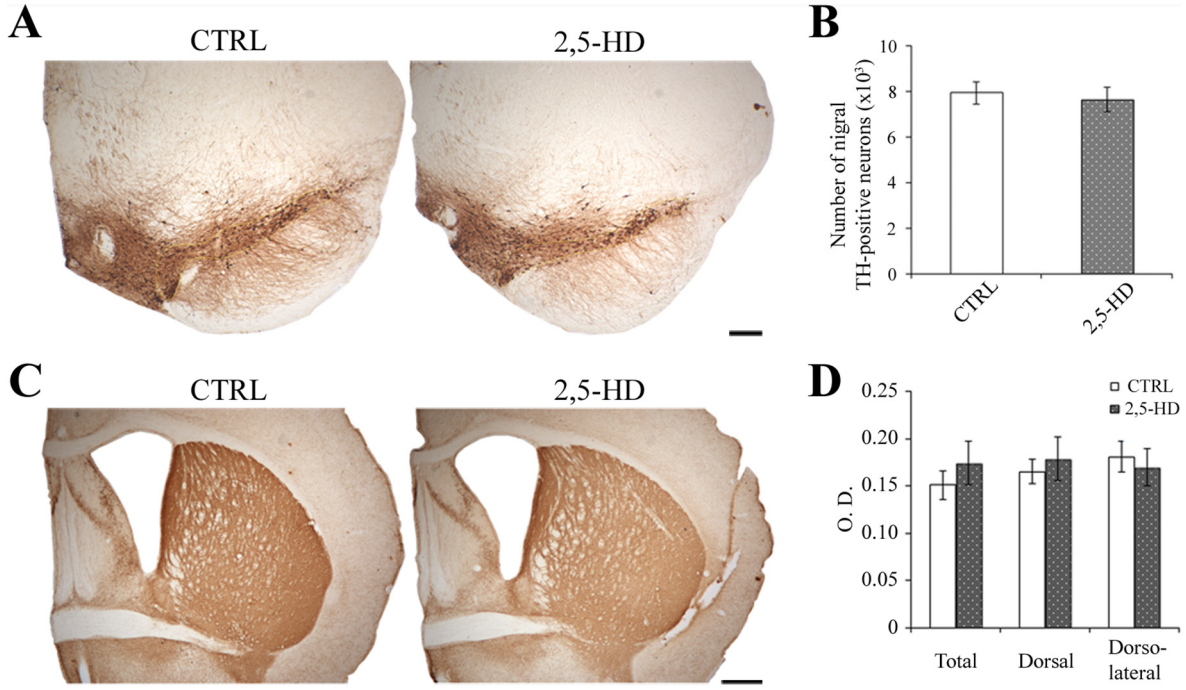

Fig. 6. 2,5-Hexanedione does not induce loss of dopaminergic neurons in *Substantia nigra pars compacta* nor the denervation of dopaminergic axonal terminals in *Corpus striatum*.

Coronal sections of *Substantia nigra pars compacta* (A) and *Corpus striatum* (C) C57BL 15-month old mice injected with saline (CTRL, left) or with 8 mmol/kg 2,5-HD for 19 days (2,5-HD, right) used for quantitative analyses of TH immunohistochemical staining (B, D). (A) Representative images of *Substantia nigra pars compacta* coronal sections used for the stereological counts of nigral TH-positive neurons. Scale bar: 100 μm. (B) Estimates of the total number of nigral TH-positive neurons in both hemispheres from mice injected with saline (CTRL, n = 8) or with 2,5-HD (2,5-HD, n = 5) calculated by stereological counts on seven coronal sections per animal throughout the *Substantia nigra pars compacta*. No differences among the groups were observed. All values are expressed as mean ± SEM. (C) Representative images of *Corpus striatum* coronal sections used for the densitometric analyses of striatal TH-positive axonal terminals. Scale bar: 500 μm. (D) Densitometric analysis of TH-positive axonal terminals in total, dorsal and dorso-lateral *Corpus striatum* of mice injected with saline (CTRL, n = 6) or with 2,5-HD (2,5-HD, n = 5) was performed on two coronal sections per animal measuring the optical density (O.D.). All values are expressed as mean ± SEM.

were observed in the presence of 2,5-HD in our experimental conditions. Accordingly, electron microscopy performed on these samples revealed a conventional ultrastructure of MTs formed in the presence of 2,5-HD (Fig. 5D). Although 2,5-HD altered the *in cell* MT system, causing the destabilization of dynamic MTs and the accumulation of stable MTs in addition to the fragmentation of total α-tubulin, it was not able to affect pure *in vitro* tubulin, meaning that the effects observed in NGF-differentiated PC12 cells could be mediated also by other proteins or that the reaction with the lysine residues needs some time to occur.

3.5. Mice injected with 2,5-hexanedione show a decreased level of tyrosinated tubulin in nigral dopaminergic neurons

Since early alterations in the MT system have already been observed in 1-methyl-4-phenyl-1,2,3,6-tetrahydropyridine (MPTP)-intoxicated mice [49], we investigated α-tubulin PTM state also in C57BL mice injected with 8 mmol/Kg of 2,5-HD for 19 consecutive days following the scheme already reported in the literature [30]. First of all, we had to assess whether there was any sign of neurodegeneration with this experimental paradigm (Fig. 6). The parameters considered to unveil the presence of neurodegeneration were: the number of dopaminergic neurons in *Substantia nigra pars compacta* and the density of their terminals projecting to the *Corpus striatum*, in particular to its dorsal part. The stereological counts of TH-positive neurons in the *pars compacta* revealed no loss of nigral dopaminergic neurons in toxin-treated mice versus controls (Fig. 6B), as shown in the representative images of midbrain coronal sections (Fig. 6A). Similarly, the immunohistochemical staining for TH and its densitometric analysis of *Corpus striatum* did not show any significant change in dopaminergic axonal terminals in total, dorsal and dorso-lateral striatum (Fig. 6C–D).

Although the selected 2,5-HD treatment was not able to induce the death of nigral dopaminergic cells or the loss of their striatal projection, we further investigated the composition of α-tubulin PTMs in three different compartments of nigrostriatal TH-positive neurons (Fig. 7A): the soma, the axons and their terminals. In order to analyse the various α-tubulin PTMs in the dopaminergic structures, sagittal brain sections were concurrently stained for TH and for tyrosinated (Fig. 7B–C), detyrosinated or acetylated tubulin (Fig. S2). Images were acquired using a confocal microscope and the fluorescence intensity of each α-tubulin PTM was measured for all neuronal compartments in the corresponding brain regions. This analysis highlighted the specific decrease of tyrosinated tubulin level in the soma of dopaminergic neurons in 2,5-HD-injected mice versus controls (Fig. 7B–C). These results are consistent with the shift of tyrosinated tubulin from polymerized to unpolymerized pool we observed in NGF-differentiated PC12 cells after 2,5-HD treatment (Fig. 5A–B) and both of them imply the destabilization of MTs.

3.6. 2,5-Hexanedione affects microtubule stability in human fibroblasts from Parkinson's disease patients

Once a general picture of the impact of the 2,5-HD action on a neuron-like cellular model and in mice had been achieved, we moved to a human system. We chose to use human skin fibroblasts, since they are considered as an easily available and robust PD experimental model [59], and because we could take advantage of the expertise already present in our lab in working with this kind of cells derived from PD patients [60]. To this purpose, the effect of 2,5-HD was tested on skin fibroblasts, obtained from healthy donors and patients harbouring

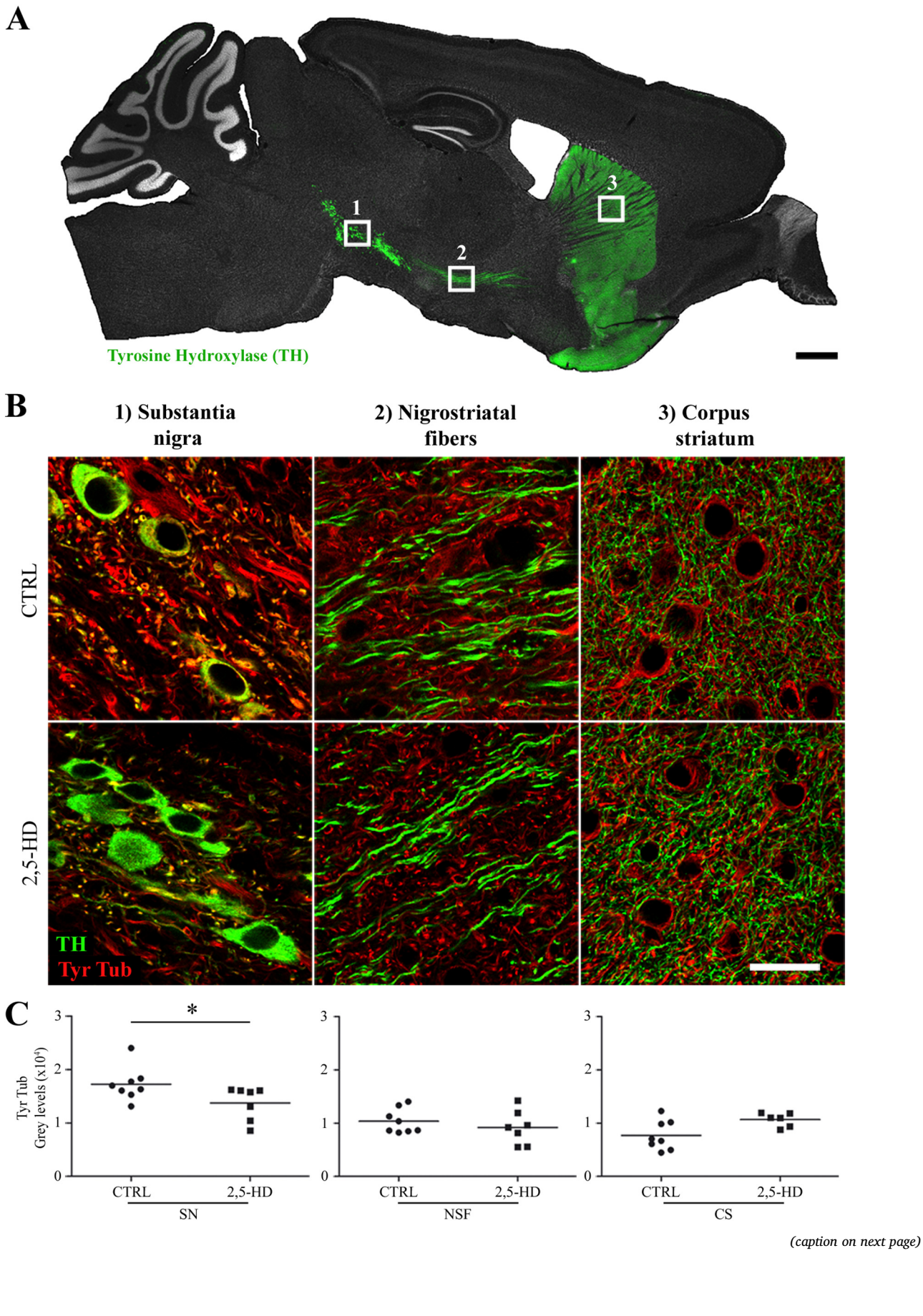

(caption on next page)

Fig. 7. Nigral dopaminergic neurons of mice injected with 2,5-hexanedione show a decreased level of tyrosinated tubulin.
(A) Overview of the nigrostriatal pathway in a sagittal section of mouse brain starting from the cell bodies of dopaminergic neurons in the *Substantia nigra pars compacta* (1, SN), passing through the nigrostriatal fibers (2, NSF) and ending with their axonal terminals in the dorsal striatum (3, CS). The brain section was stained for tyrosine hydroxylase (TH, green), marker of dopaminergic neurons, together with DAPI (grey) to visualize the nuclei. Scale bar: 500 μm. (B) Representative confocal images and (C) fluorescence intensity analyses of different regions of dopaminergic neurons from three areas of nigrostriatal pathway in C57BL 15-month old mice treated with saline (CTRL) or with 2,5-HD (8 mmol/kg for 19 days, 2,5-HD): the neuronal bodies in *Substantia nigra pars compacta* (1), the nigrostriatal fibers (2) and the axonal terminals in *Corpus striatum* (3). (B) The green signal represents the tyrosine hydroxylase (TH) staining, while the red signal is the tyrosinated tubulin (Tyr Tub). Scale bar: 20 μm. (C) Quantification of fluorescence intensity of tyrosinated tubulin (Tyr Tub) in dopaminergic neurons in three different areas of the nigrostriatal pathway in sagittal sections of mice treated with saline (CTRL, n = 8) or with 2,5-HD (2,5-HD, n = 7). Data are expressed in grey levels using dot plots, with every dot representing the mean fluorescence intensity value per animal. *$p < 0.05$ vs control group (CTRL) according to Mann-Whitney *U* test. (For interpretation of the references to colour in this figure legend, the reader is referred to the web version of this article.)

Table 2
Phenotype and genotype characterization of investigated individuals.

	Code	Genotype	Sex	Age of biopsy	Age of onset
Healthy donors	FFF0422011		M	69	
	FFF0521978		M	51	
	FFF0531978		F	44	
PD patients (*PRKN*)	FFF0142009	c.C924T (p.R275W);exon 3 del.	F	41	22
	FFF0292009	exon 3 del (homozygotes)	F	69	39
	FFF0902009	c.del202_203AG (p.Q34/X43) (homozygotes)	M	51	20

The characteristics present in the table are: the identification code; the genotype (just for PD patients); the sex; the age at time of skin biopsy and establishment of fibroblast cell line; the age at which the patient first noticed a PD-related symptom (that was considered the age at onset of the disease).

mutations in *PRKN* (Table 2), a specific PD-related gene coding for Parkin, an ubiquitin E3 ligase [61] also able to bind and stabilize MTs [35,62]. At this point, we wanted to evaluate whether 2,5-HD could have an effect on MT destabilization that has been previously described in PD patient fibroblasts [60]. After 24 hour-exposure to 2,5-HD, we observed that both cell viability and morphology were not affected by the treatment (Fig. 8A–D). Nevertheless, in baseline conditions differences in fibroblasts from PD patients and healthy subjects were seen in terms of morphology, since they were wider and larger (Fig. 8A), had a larger cell area (Fig. 8C) and a significantly lower ratio between maximum and minimum axis (Fig. 8D), as shown by the present morphometric analyses and according to our previous work [60].

To assess the effect of 2,5-HD on MT stability in human fibroblasts, the state of tubulin polymerization was analysed as well. As previously reported [60], we confirmed that MT destabilization was present in patients already at baseline without the addition of any stressor, then we observed that 2,5-HD treatment was able to induce stabilization of MTs only in PD patient cells (Fig. 8E–F). Interestingly, MT stabilization occurred already at the lowest dose of 2,5-HD in PD fibroblasts, whereas healthy ones were not affected at all, suggesting greater MT frailty in PD patient cells. These data show that 2,5-HD impacts MT stability both in neuron-like cells and in human fibroblasts. It is noteworthy that they also suggest that the genetic background may really make a difference in terms of MT susceptibility to this environmental PD toxin.

4. Discussion

In this work, we focused on MT cytoskeleton, since there is a growing body of evidence supporting its dysfunction in the pathogenesis of several neurological diseases including PD [63–65]. Here, we demonstrate for the first time that MT dysfunction occurs in 2,5-HD-induced neurodegeneration, a finding that is consistent with the impairment of MT stability and α-tubulin PTMs already found in MPTP-intoxicated mice [49], in human skin fibroblasts derived from PD patients [60] and even in mesenchymal stromal cells of patients with Progressive Supranuclear Palsy [66], a rare neurodegenerative disorder associated with both dementia and parkinsonism.

Several lines of evidence have shown that mitochondrial dysfunction is a key element in the pathogenesis of PD [67] and that is why mitochondria have been in the spotlight of the scientific community for many years. Recently, Qi and colleagues [68] exhaustively analysed the effects of 2,5-HD on mitochondria-related pathways in undifferentiated PC12 cells, showing that toxin-induced apoptosis occurs via mitochondria-induced activity of Caspase-3. Moreover, all these 2,5-HD-induced alterations were successfully prevented by treatment with the anti-oxidant taurine [69]. Unfortunately, the authors did not look at any components of the cytoskeleton in undifferentiated cells, so we cannot really compare the respective role of mitochondria- and MT-based effects in triggering cell death. Nevertheless, Malorni and colleagues [54] already demonstrated that 2,5-HD interferes with cell proliferation, reporting that cells detached from the substrate when they were in the mitotic phase after treatment. Accordingly, the toxin induces significant mortality of undifferentiated PC12 cells [68], whereas treating NGF-differentiated PC12 cells with comparable concentrations of 2,5-HD did not induce any significant cell death. This is a clue supporting the direct action of 2,5-HD on MTs, since they are responsible for the assembly/disassembly of the mitotic spindle and suggesting why cell viability was not affected in non-dividing cells, such as neurons. Therefore, we analysed the neurotoxic action of 2,5-HD more accurately in 5-day NGF-differentiated PC12 cells, since they are an established neuronal model. In this model we reported that the formation of varicosities along neurites were already evident at 2 mM of toxin and even more striking the increased number of differentiated cells with perinuclear accumulation of stable MTs already at 0.2 mM, when the loss of cell viability, mitochondrial alterations and autophagy activation were not yet detectable. This finding suggests that mitochondria are unlikely to be the first target of 2,5-HD. A consistent finding was that also healthy fibroblasts exposed to 2.8 mM 2,5-HD underwent changes in their morphology after 3 days of treatment, showing a large swollen cell body and thin elongated processes [70]. In fact, alterations in cell shape typically depend on the cytoskeleton and, in particular, on MT functionality, with a possible block of the axonal transport leading to accumulation of proteins and organelles.

Abnormal accumulations of NFs have been detected in many human neurodegenerative disorders, including amyotrophic lateral sclerosis, Alzheimer's disease, PD and Charcot-Marie-Tooth disease [71]. The effects of 2,5-HD on intermediate filaments have been extensively described in many previous studies, but MTs have been poorly investigated. By immunocytochemical approach, we highlighted the presence of NF accumulation inside the axonal swellings and in the perinuclear area in NGF-differentiated PC12 cells, a finding that is consistent with data obtained in other cellular models [27,55,56,72] and in patients showing distal axonal accumulation of NFs [73,74]. Meanwhile, we observed the significant reduction in NF levels by immunoblotting as seen also in rat dorsal root ganglia cells [31] and in the nervous system of intoxicated rats [75,76]. Similarly, in NGF-differentiated PC12 cells fluorescence staining highlighted a partial fragmentation of the MT network and, surprisingly, perinuclear

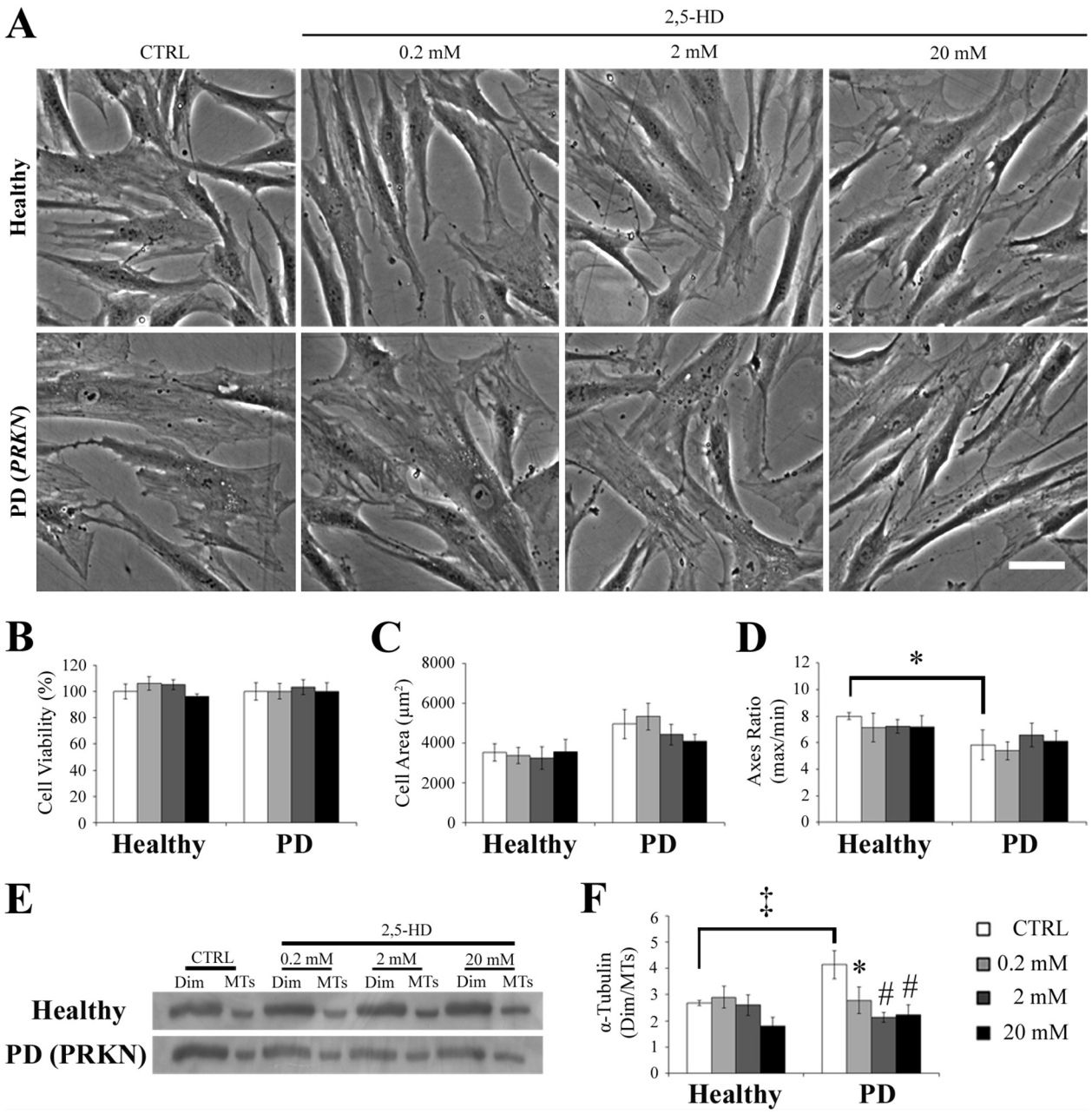

Fig. 8. 2,5-Hexanedione affects microtubule stability in human fibroblasts from Parkinson's disease patients.
(A) Representative phase contrast images of cultured human skin fibroblasts of healthy and PD-affected individuals treated for 24 h with different concentrations of 2,5-HD. Scale bar: 50 μm. (B) Cell viability, evaluated by MTT test, was not affected in both groups by the toxin. (C–D) Morphometric analyses showed an increased area (C) and a significantly reduced ratio between maximum and minimum axis (D) in fibroblasts of patients harbouring mutations in *PRKN* gene. All values are expressed as mean ± SEM. *$p < 0.05$ vs healthy fibroblast control group (CTRL) according to according to Mann-Whitney U test. (E–F) Triton-X100-soluble (representing the α-tubulin dimer pool, Dim) and -insoluble fraction (α-tubulin incorporated into microtubules, MTs) of human skin fibroblasts were analysed by (E) immunoblot and (F) densitometric analyses, shown as ratio between free dimers and microtubules. The genetic background influences the tubulin distribution between the two fractions already at the baseline condition. The PD fibroblasts resulted much more susceptible to the action of 2,5-HD, in fact, the ratio was shifted towards the microtubule fraction even at lower doses of toxin. All values are expressed as mean ± SEM. $^{‡}p < 0.05$ vs healthy control (CTRL) according to one-way ANOVA, Fisher LSD post hoc test; *$p < 0.05$ and $^{\#}p < 0.01$ vs PD control group (CTRL) according to one-way ANOVA, Fisher LSD post hoc test.

accumulation of stable MTs, just like NFs. To our knowledge, this MT accumulation has never been observed before, probably because the particular structure of dopaminergic neurons makes them particularly susceptible to toxins that impact on MTs, whereas in other cell types this effect could be masked and underestimated. On the other hand, the MT fragmentation along the axons could be connected to the already known action of some anti-cancer drugs, which exerted adverse effects on the peripheral nervous system in clinical studies, with documentation of degeneration and fragmentation of sensory axons, reduced axonal length and also reduced axonal transport in animal models [77]. Interestingly, it has recently been reported that intermediate filament accumulation directly alters MT stability in motor neurons in *Caenorhabditis elegans* [78]. Kurup and colleagues showed for the first time that the genetic loss or the pharmacological disruption of the essential intermediate filament network was sufficient to shift the MT balance from stable to dynamic, participating in the regulation of axonal transport, from which synapse rewiring depends in *C. elegans*. Actually, 2,5-HD acts directly on both intermediate filaments and MTs, but to a

different extent, possibly due to the different intracellular amount of the two types of filaments, since NFs account for up to 85% of the total protein of fully differentiated neurons [79], making it difficult to define the specific contribution of NFs and MTs to the final effect.

MTs show a dynamic behaviour, switching rapidly between growth and depolymerisation phases, but there is a limited range of acceptable MT dynamic behaviours in neurons, outside of which MTs cannot function normally and the cells cannot survive [80]. Indeed, both reduced or increased MT stability can lead to neurodegeneration [77]. Since PTMs of tubulin have been correlated to stability of MT cytoskeleton for a long time and are currently considered crucial regulators of its functions, they have a strong potential to be implicated in a number of disorders. For example, mice lacking tubulin-tyrosine ligase activity show strongly upregulated levels of detyrosinated tubulin in the brain and die perinatally due to massive defects in brain architecture [81], while axonal transport defects have been linked to decreased tubulin acetylation in various neurodegenerative diseases, including PD [82]. Interestingly, we observed a specific imbalance of modified forms of α-tubulin in NGF-differentiated PC12 cells after toxin exposure. Worthy of note, all the three PTMs analysed were significantly affected by 2,5-HD and changed in level, distribution or both. Here, we showed different types of toxin effects on MT system. First, a MT stabilizing effect suggested by the increased levels of detyrosinated tubulin, associated to stable MTs, and its perinuclear accumulation together with the decreased levels of tyrosinated tubulin, marker of native and dynamic MT pool. Second, the analysis of tubulin polymerization in NGF-differentiated PC12 cells revealed the imbalance of tyrosinated tubulin ratio between dimers and MTs, showing that 2,5-HD caused the reduction in the dynamic MT fraction, suggesting MT destabilization. An alteration in MT stability was also found *in vivo* in dopaminergic neurons in *Substantia nigra pars compacta* of mice intoxicated with 2,5-HD. Similarly, the amount of dynamic MTs was significantly reduced in the soma of nigral dopaminergic neurons. Surprisingly, acetylated MTs were affected by the treatment in terms of distribution, but their level remained unchanged. Since acetylation is known to happen on lysine 40 of α-tubulin, making MTs more resistant to mechanical stress [83,84], we can guess that also 2,5-HD may be able to interact with the same free lysine residues competing for the binding. From this standpoint, it is possible that in 2,5-HD models the acetylated MTs are not an appropriate marker to analyse toxin effects inasmuch they could be underestimated. In addition, 2,5-HD treatment was able to alter MT stability also in human skin fibroblasts from PD patients harbouring mutations in *PRKN* gene already at the lowest dose of toxin, but not in the healthy ones, revealing how genetic background and environment can interact in impacting MT system in pathological conditions. Consistently with this, but even more strikingly, it has been shown that also a particular mitochondrial DNA background can increase the sensitivity to 2,5-HD toxicity, triggering the onset of Leber's hereditary optic neuropathy (LHON) in cybrids and fibroblasts harbouring mutation in *LHON* gene [85]. These data strongly suggest that the genetic background may really make a difference in MT susceptibility to environmental factors, such as this PD toxin. Hence, the contribution of environmental toxins to the study of neurodegeneration diseases is revaluated in terms of potential dissection of the various neurodegenerative pathways.

4.1. Conclusions

In conclusion, our data support the hypothesis that MT system impairment is an early and crucial event in the 2,5-HD-induced neurodegeneration of the dopaminergic system, suggesting that MT dysfunction may have a key role in the process leading neurons to death. Therefore, it could be a good target for new neuroprotective drugs. The use of MT-stabilizing agents, such as epothilone D, holds promise in animal models of neurodegeneration [49,86]. Unfortunately, a clinical trial on patients with mild Alzheimer's disease was discontinued due to the appearance of adverse side effects [87]. On the other hand, alteration of tubulin PTMs could be a risk factor and a new biomarker for specific disorders, indicating reduced protection against potential disease-causing insults, such as 2,5-HD. Among the various enzymes responsible for the various modifications, HDAC6 inhibition is able to rescue pathological phenotype in many different neurodegenerative models [82,88,89], making it the most promising option for the treatment of neurodegeneration, so much so that in 2018 a Phase I clinical trial was started with the aim of evaluating the safety, tolerability and pharmacokinetics of CKD-504 (a selective HDAC6 inhibitor) in Huntington's disease patients [90]. Consequently, the modulation of tubulin PTMs offers new hope for the treatment of neurodegenerative diseases, including PD.

Transparency document

The Transparency document associated this article can be found, in online version.

Acknowledgements

Fondazione Grigioni per il Morbo di Parkinson (Milan, Italy) supported this research (grant to GC) and the fellowship to FVMC and AMC. The authors thank “Cell Line and DNA Biobank from Patients affected by Genetic Diseases” (Istituto G. Gaslini, Genoa, Italy) and the “Parkinson Institute Biobank” (Milan, Italy), members of the Telethon Network of Genetic Biobanks (project no. GTB12001) funded by Telethon (Italy), and Dr. Stefano Goldwurm (Parkinson Institute, ASST Gaetano Pini-CTO, Milan, Italy) for supplying human fibroblast cell lines. The authors thank Dr. Jennifer S. Hartwig for reading and editing the manuscript. The authors are grateful to Dr. Michela Signo, Dr. Michele Cassano, Dr. Nagiua Haymour, Dr. Martina Ferrari and Dr. Kristyna Hanusova for the technical support and their help in the lab (Department of Biosciences, University of Milan, Milan, Italy). The authors also thank Dr. Dario Parazzoli (Imaging Technological Development Unit in IFOM, the FIRC Institute of Molecular Oncology, Milan, Italy) for the use of Leica TCS SP5 confocal laser scanning microscope. Finally, the authors apologize for each possible involuntary paper omission.

Authorship

FVMC, GP and GC conceived and designed the experiments. FVMC performed all the experiments on PC12 cells and human fibroblasts, in addition to optical microscopy analysis on cells. FVMC and AMC performed protein analysis by Western blotting. FVMC, AA, DC and DM performed *in vivo* experiments and processed mouse brain sections for immunofluorescence and immunochemical stainings. FVMC and DM performed the stereological counts of TH-positive cells. FVMC performed the densitometric analysis on striatal sections. FVMC, DC, IC and MA performed the confocal microscopy analysis. FVMC and DC performed *in vitro* assays. FC, EO and AM performed electron microscopy analysis. FVMC analysed the data. FVMC and GC wrote the paper. All the authors carefully reviewed and approved the final manuscript.

About research data

The datasets generated during and/or analysed during the current study are available from the corresponding author on reasonable request.

Appendix A. Supplementary data

Supplementary data to this article can be found online at https://doi.org/10.1016/j.bbadis.2019.165581.

References

[1] W. Dauer, S. Przedborski, Parkinson's disease: mechanisms and models, Neuron. 39 (2003) 889–909.
[2] J.A. Obeso, M.C. Rodriguez-Oroz, C.G. Goetz, C. Marin, J.H. Kordower, M. Rodriguez, E.C. Hirsch, M. Farrer, A.H.V. Schapira, G. Halliday, Missing pieces in the Parkinson's disease puzzle, Nat. Med. 16 (2010) 653–661.
[3] J.M. Vance, S. Ali, W.G. Bradley, C. Singer, D. a Di Monte, Gene-environment interactions in Parkinson's disease and other forms of parkinsonism, Neurotoxicology. 31 (2010) 598–602.
[4] S.M. Fleming, Mechanisms of gene-environment interactions in Parkinson's disease, Curr. Environ. Health. Rep. 4 (2017) 192–199.
[5] D.A. Di Monte, M. Lavasani, A.B. Manning-bog, Environmental factors in Parkinson's disease, 23 (2002) 487–502.
[6] J.M. Hatcher, K.D. Pennell, G.W. Miller, Parkinson's disease and pesticides: a toxicological perspective, Trends Pharmacol. Sci. 29 (2008) 322–329.
[7] E.A. Lock, J. Zhang, H. Checkoway, Solvents and Parkinson disease: a systematic review of toxicological and epidemiological evidence, Toxicol. Appl. Pharmacol. 266 (2013) 345–355.
[8] G. Pezzoli, S. Barbieri, C. Ferrante, A. Zecchinelli, V. Foà, Parkinsonism due to n-hexane exposure, lancet, The. 2 (1989) 874.
[9] G. Pezzoli, A. Antonini, S. Barbieri, M. Canesi, L. Perbellini, A. Zecchinelli, C.B. Mariani, A. Bonetti, K.L. Leenders, n-Hexane-induced parkinsonism: pathogenetic hypotheses, Mov. Disord. 10 (1995) 279–282.
[10] G. Pezzoli, O. Stada, V. Silani, A. Zecchinelli, L. Perbellini, F. Javoy-Agid, P. Ghidoni, E.D. Motti, T. Masini, G. Scarlato, Y. Agid, E.C. Hirsch, Clinical and pathological features in hydrocarbon-induced parkinsonism, Ann. Neurol. 40 (1996) 922–925.
[11] G. Pezzoli, M. Canesi, A. Antonini, A. Righini, L. Perbellini, M. Barichella, C.B. Mariani, F. Tenconi, S. Tesei, A. Zecchinelli, K.L. Leenders, Hydrocarbon solvent exposure and Parkinson disease, Neurology. 55 (2000) 667–673.
[12] N. Vanacore, M. Gasparini, L. Brusa, G. Meco, A possible association between exposure to n-hexane and parkinsonism, Neurol. Sci. 21 (2000) 49–52.
[13] M. Canesi, R. Benti, G. Marotta, R. Cilia, I.U. Isaias, P. Gerundini, G. Pezzoli, A. Antonini, Striatal dopamine transporter binding in patients with Parkinson's disease and severe occupational hydrocarbon exposure, Eur. J. Neurol. 14 (2007) 297–299.
[14] G. Pezzoli, E. Cereda, Exposure to pesticides or solvents and risk of Parkinson disease, Neurology. 80 (2013) 2035–2041.
[15] R.M. LoPachin, T. Gavin, Toxic neuropathies: mechanistic insights based on a chemical perspective, Neurosci. Lett. 596 (2015) 78–83.
[16] G.D. Hammond-Tooke, Slow axonal transport is impaired by intrathecal 2,5-hexanedione, Exp. Neurol. 116 (1992) 210–217.
[17] P.S. Spencer, H.H. Schaumburg, M.I. Sabri, B. Veronesi, The enlarging view of hexacarbon neurotoxicity, Crit. Rev. Toxicol. 7 (1980) 279–356.
[18] G. Pezzoli, S. Ricciardi, C. Masotto, C.B. Mariani, A. Carenzi, n-Hexane induces parkinsonism in rodents, Brain Res. 531 (1990) 355–357.
[19] C. Masotto, C. Bisiani, C. Camisasca, R. Fusi, S. Ricciardi, N. Fonzi, L. Perbellini, M. Scatturin, C. Mariani, M. Canesi, Effects of acute n-hexane and 2,5-hexanedione treatment on the striatal dopaminergic system in mice, J. Neural Transm. Suppl. 45 (1995) 281–285.
[20] C. Zhang, L. Hou, J. Yang, Y. Che, F. Sun, H. Li, Q. Wang, 2,5-Hexanedione induces dopaminergic neurodegeneration through integrin αMβ2/NADPH oxidase axis-mediated microglial activation, Cell Death Dis. 9 (2018) 60.
[21] M. Canesi, L. Perbellini, L. Maestri, a Silvani, L. Zecca, L. Bet, G. Pezzoli, Poor metabolization of n-hexane in Parkinson's disease., J. Neurol. 250 (2003) 556–60. doi:https://doi.org/10.1007/s00415-003-1035-y.
[22] N. Fedtke, H.M. Bolt, Detection of 2,5-hexanedione in the urine of persons not exposed to n-hexane, Int. Arch. Occup. Environ. Health 57 (1986) 143–148.
[23] P. Bavazzano, P. Apostoli, C. Balducci, G.B. Bartolucci, M. Buratti, P. Duca, G. Gori, V. Li Donni, L. Perbellini, A. Perico, C. Minoia, Determination of urinary 2,5-hexanedione in the general Italian population, Int. Arch. Occup. Environ. Health 71 (1998) 284–288, https://doi.org/10.1007/s004200050282.
[24] B. Persson, M. Vrethem, N. Murgia, J. Lindh, A.L. Hällsten, M. Fredrikson, M. Tondel, Urinary 2,5-hexanedione excretion in cryptogenic polyneuropathy compared to the general Swedish population, J. Occup. Med. Toxicol. 8 (2013) 21.
[25] P. Xing-Fu, Q. Ya-Ling, Z. Wei, T. Hong-Fang, R. Zheng, W. Bang-Hua, H. Han-Lin, Z. Yu-Xin, Y. Hui-Fang, Determination of total urinary 2,5-hexanedione in the Chinese general population, Environ. Res. 150 (2016) 645–650.
[26] L. Perbellini, G. Pezzoli, F. Brugnone, M. Canesi, Biochemical and physiological aspects of 2, 5-hexanedione: endogenous or exogenous product?, 65 (1993) 49–52.
[27] D.G. Graham, V. Amarnath, W.M. Valentine, S.J. Pyle, D.C. Anthony, Pathogenetic studies of hexane and carbon disulfide neurotoxicity, Crit. Rev. Toxicol. 25 (1995) 91–112.
[28] R.M. LoPachin, A.P. DeCaprio, γ-Diketone neuropathy: axon atrophy and the role of cytoskeletal protein adduction, Toxicol. Appl. Pharmacol. 199 (2004) 20–34.
[29] J.D. Stone, A.P. Peterson, J. Eyer, T.G. Oblak, D.W. Sickles, Axonal neurofilaments are nonessential elements of toxicant-induced reductions in fast axonal transport: video-enhanced differential interference microscopy in peripheral nervous system axons, Toxicol. Appl. Pharmacol. 161 (1999) 50–58.
[30] J.D. Stone, A.P. Peterson, J. Eyer, T.G. Oblak, D.W. Sickles, Neurofilaments are nonessential to the pathogenesis of toxicant-induced axonal degeneration, J. Neurosci. 21 (2001) 2278–2287.
[31] X.-Y. Han, D. Cheng, F.-Y. Song, T. Zeng, L.-H. An, K.-Q. Xie, Decelerated transport and its mechanism of 2,5-hexanedione on middle-molecular-weight neurofilament in rat dorsal root ganglia cells, Neuroscience. 269 (2014) 192–198.
[32] K. Boekelheide, 2,5-Hexanedione alters microtubule assembly I, Toxicol. Appl. Pharmacol. 88 (1987) 370–382.
[33] M.A. Alim, M.S. Hossain, K. Arima, K. Takeda, Y. Izumiyama, M. Nakamura, H. Kaji, T. Shinoda, S. Hisanaga, K. Ueda, Tubulin seeds alpha-synuclein fibril formation, J. Biol. Chem. 277 (2002) 2112–2117.
[34] F. Gillardon, Leucine-rich repeat kinase 2 phosphorylates brain tubulin-beta isoforms and modulates microtubule stability - a point of convergence in Parkinsonian neurodegeneration? J. Neurochem. 110 (2009) 1514–1522.
[35] Y. Ren, J. Zhao, J. Feng, Parkin binds to alpha/beta tubulin and increases their ubiquitination and degradation, J. Neurosci. 23 (2003) 3316–3324.
[36] G. Cappelletti, M.G. Maggioni, R. Maci, Influence of MPP + on the state of tubulin polymerisation in NGF-differentiated PC12 cells, J. Neurosci. Res. 56 (1999) 28–35.
[37] B.R. Brinkley, S.S. Barham, S.C. Barranco, G.M. Fuller, Rotenone inhibition of spindle microtubule assembly in mammalian cells, Exp. Cell Res. 85 (1974) 41–46.
[38] S. Millecamps, J.-P. Julien, Axonal transport deficits and neurodegenerative diseases, Nat. Rev. Neurosci. 14 (2013) 161–176.
[39] K.J. De Vos, A.J. Grierson, S. Ackerley, C.C.J. Miller, Role of axonal transport in neurodegenerative diseases, Annu. Rev. Neurosci. 31 (2008) 151–173.
[40] S. Gadadhar, S. Bodakuntla, K. Natarajan, C. Janke, The tubulin code at a glance, J. Cell Sci. 130 (2017) 1347–1353.
[41] M.M. Magiera, P. Singh, S. Gadadhar, C. Janke, Tubulin posttranslational modifications and emerging links to human disease, Cell. 173 (2018) 1323–1327.
[42] A. Hughes, What features improve the accuracy of clinical diagnosis in Parkinson's disease, Neurology. 42 (1992) 1142–1146.
[43] F. Sironi, P. Primignani, M. Zini, S. Tunesi, C. Ruffmann, S. Ricca, T. Brambilla, A. Antonini, S. Tesei, M. Canesi, A. Zecchinelli, C. Mariani, N. Meucci, G. Sacilotto, R. Cilia, I.U. Isaias, B. Garavaglia, D. Ghezzi, M. Travi, A. Decarli, D. a Coviello, G. Pezzoli, S. Goldwurm, Parkin analysis in early onset Parkinson's disease, Park. Relat. Disord. 14 (2008) 326–333.
[44] M. Yamazaki, K. Chiba, T. Mohri, H. Hatanaka, Cyclic GMP-dependent neurite outgrowth by genipin and nerve growth factor in PC12h cells, Eur. J. Pharmacol. 488 (2004) 35–43.
[45] A. Grünewald, L. Voges, A. Rakovic, M. Kasten, H. Vandebona, C. Hemmelmann, K. Lohmann, S. Orolicki, A. Ramirez, A.H.V. Schapira, P.P. Pramstaller, C.M. Sue, C. Klein, Mutant parkin impairs mitochondrial function and morphology in human fibroblasts, PLoS One 5 (2010) e12962.
[46] G. Cappelletti, M.G. Maggioni, G. Tedeschi, R. Maci, Protein tyrosine nitration is triggered by nerve growth factor during neuronal differentiation of PC12 cells, Exp. Cell Res. 288 (2003) 9–20.
[47] M. Castoldi, A.V. Popov, Purification of brain tubulin through two cycles of polymerization-depolymerization in a high-molarity buffer, Protein Expr. Purif. 32 (2003) 83–88.
[48] A. Contini, G. Cappelletti, D. Cartelli, G. Fontana, M.L. Gelmi, Molecular dynamics and tubulin polymerization kinetics study on 1,14-heterofused taxanes: evidence of stabilization of the tubulin head-to-tail dimer-dimer interaction, Mol. BioSyst. 8 (2012) 3254–3261.
[49] D. Cartelli, F. Casagrande, C.L. Busceti, D. Bucci, G. Molinaro, A. Traficante, D. Passarella, E. Giavini, G. Pezzoli, G. Battaglia, G. Cappelletti, Microtubule alterations occur early in experimental parkinsonism and the microtubule stabilizer epothilone D is neuroprotective, Sci. Rep. 3 (2013) 1837.
[50] K. Franklin, G. Paxinos, The Mouse Brain in Stereotaxic Coordinates, Elsevier, Third Edit, 2007.
[51] L.A. Greene, A.S. Tischler, Establishment of a noradrenergic clonal line of rat adrenal pheochromocytoma cells which respond to nerve growth factor, Proc. Natl. Acad. Sci. U. S. A. 73 (1976) 2424–2428.
[52] K. a Malkus, E. Tsika, H. Ischiropoulos, Oxidative modifications, mitochondrial dysfunction, and impaired protein degradation in Parkinson's disease: how neurons are lost in the Bermuda triangle, Mol. Neurodegener. 4 (2009) 24.
[53] I. Scott, R. j. Youle, Mitochondrial fission and fusion, Essays Biochem. (2010) 85–98.
[54] W. Malorni, F. Iosi, G. Formisano, G. Arancia, Cytoskeletal changes induced in vitro by 2,5-hexanedione: an immunocytochemical study, Exp. Mol. Pathol. 50 (1989) 50–68.
[55] C.L. Hartley, V.E. Anderson, B.H. Anderton, J. Robertson, B.H. Anderson, Acrylamide and 2,5-hexanedione induce collapse of neurofilaments in SH-SY5Y human neuroblastoma cells to form perikaryal inclusion bodies, Neuropathol. Appl. Neurobiol. 23 (1997) 364–372.
[56] E. Heijink, P. Bolhuis, F. De Wolff, Sensitivity to 2,5-hexanedione of neurofilaments in neuroblastoma cell line SK-N-SH increases during differentiation, J. Neuropathol. Exp. Neurol. 54 (1995) 82–90.
[57] F. Francis, S. Roy, S.T. Brady, M.M. Black, Transport of neurofilaments in growing axons requires microtubules but not actin filaments, J. Neurosci. Res. 79 (2005) 442–450.
[58] C. Janke, The tubulin code: molecular components, readout mechanisms, and functions, J. Cell Biol. 206 (2014) 461–472.
[59] G. Auburger, M. Klinkenberg, J. Drost, K. Marcus, B. Morales-Gordo, W.S. Kunz, U. Brandt, V. Broccoli, H. Reichmann, S. Gispert, M. Jendrach, Primary skin fibroblasts as a model of Parkinson's disease, Mol. Neurobiol. 46 (2012) 20–27.
[60] D. Cartelli, S. Goldwurm, F. Casagrande, G. Pezzoli, G. Cappelletti, Microtubule destabilization is shared by genetic and idiopathic Parkinson's disease patient fibroblasts, PLoS One 7 (2012) e37467.
[61] H. Shimura, N. Hattori, S.I. Kubo, Y. Mizuno, S. Asakawa, S. Minoshima, N. Shimizu, K. Iwai, T. Chiba, K. Tanaka, T. Suzuki, Familial Parkinson disease gene product, parkin, is a ubiquitin-protein ligase, Nat. Genet. 25 (2000) 302–305.
[62] F. Yang, Q. Jiang, J. Zhao, Y. Ren, M.D. Sutton, J. Feng, Parkin stabilizes

microtubules through strong binding mediated by three independent domains, J. Biol. Chem. 280 (2005) 17154–17162.
[63] D. Cartelli, G. Cappelletti, Microtubule destabilization paves the way to Parkinson's disease, Mol. Neurobiol. 54 (2017) 6762–6774.
[64] L. Pellegrini, A. Wetzel, S. Grannó, G. Heaton, K. Harvey, Back to the tubule: microtubule dynamics in Parkinson's disease, Cell. Mol. Life Sci. 74 (2017) 409–434.
[65] S. Chakraborti, K. Natarajan, J. Curiel, C. Janke, J. Liu, The emerging role of the tubulin code: from the tubulin molecule to neuronal function and disease, Cytoskeleton. 73 (2016) 521–550.
[66] A.M. Calogero, M. Viganò, S. Budelli, D. Galimberti, C. Fenoglio, D. Cartelli, L. Lazzari, P. Lehenkari, M. Canesi, R. Giordano, G. Cappelletti, G. Pezzoli, Microtubule defects in mesenchymal stromal cells distinguish patients with Progressive Supranuclear Palsy, J. Cell. Mol. Med. 22 (2018) 2670–2679.
[67] W. Poewe, K. Seppi, C.M. Tanner, G.M. Halliday, J. Volkmann, A. Schrag, A.E. Lang, Parkinson disease, Nat. Rev. Dis. Prim. 3 (2017) 17013.
[68] Y. Qi, S. Li, F. Piao, Z. Wang, R. Chen, S. Liu, J. Shen, 2,5-Hexanedione induces apoptosis via a mitochondria-mediated pathway in PC12 cells, Mol. Cell. Toxicol. 11 (2015) 79–87.
[69] S. Li, H. Guan, Z. Qian, Y. Sun, C. Gao, G. Li, Y. Yang, F. Piao, S. Hu, Taurine inhibits 2,5-hexanedione-induced oxidative stress and mitochondria-dependent apoptosis in PC12 cells, Ind. Health 55 (2017) 108–118.
[70] M. Passarin, S. Monaco, S. Ferrari, C. Giannini, N. Rizzuto, G. Moretto, Cytoskeletal changes in cultured human fibroblasts following exposure to 2,5-hexanedione, Neuropathol. Appl. Neurobiol. 22 (1996) 60–67.
[71] R. Perrot, R. Berges, A. Bocquet, J. Eyer, Review of the multiple aspects of neurofilament functions, and their possible contribution to neurodegeneration, Mol. Neurobiol. 38 (2008) 27–65.
[72] D. Tuckwell, L. Laszlo, R. Mayer, 2,5-Hexanedione-induces intermediate filament aggregates contain ubiquitin-protein conjugate immunoreactivity and resemble Rosenthal fibres, Neuropathol. Appl. Neurobiol. 18 (1992) 593–609.
[73] A. Herskowitz, N. Ishii, H. Schaumburg, n-Hexane neuropathy a syndrome occurring as a result of industrial exposure, N. Engl. J. Med. 285 (1971) 82–85.
[74] R. Scelsi, S.M. Candura, Neuropatie tossiche occupazionali: quadri morfologici in biopsie del nervo periferico, G. Ital. Med. Lav. 34 (2012) 410–419.
[75] F. Song, C. Zhang, S. Yu, X. Zhao, L. Yu, K. Xie, Time-dependent alteration of cytoskeletal proteins in cerebral cortex of rat during 2,5-hexanedione-induced neuropathy, Neurochem. Res. 32 (2007) 1407–1414.
[76] Q.-S. Wang, L.-Y. Hou, C.-L. Zhang, F.-Y. Song, K.-Q. Xie, Changes of cytoskeletal proteins in nerve tissues and serum of rats treated with 2,5-hexanedione, Toxicology. 244 (2008) 166–178.
[77] J. Dubey, N. Ratnakaran, S.P. Koushika, Neurodegeneration and microtubule dynamics: death by a thousand cuts, Front. Cell. Neurosci. 9 (2015) 343.
[78] N. Kurup, Y. Li, A. Goncharov, Y. Jin, Intermediate filament accumulation can stabilize microtubules in Caenorhabditis elegans motor neurons, Proc. Natl. Acad. Sci. U. S. A. 115 (2018) 3114–3119.
[79] W.J. Griffin, D.F. Watson, Axonal transport in neurological disease, Ann. Neurol. 23 (1988) 3–13.
[80] S.C. Feinstein, L. Wilson, Inability of tau to properly regulate neuronal microtubule dynamics: a loss-of-function mechanism by which tau might mediate neuronal cell death, Biochim. Biophys. Acta 1739 (2005) 268–279.
[81] C. Erck, L. Peris, A. Andrieux, C. Meissirel, A.D. Gruber, M. Vernet, A. Schweitzer, Y. Saoudi, H. Pointu, C. Bosc, P.A. Salin, D. Job, J. Wehland, A vital role of tubulin-tyrosine-ligase for neuronal organization, Proc. Natl. Acad. Sci. U. S. A. 102 (2005) 7853–7858.
[82] V.K. Godena, N. Brookes-Hocking, A. Moller, G. Shaw, M. Oswald, R.M. Sancho, C.C.J. Miller, A.J. Whitworth, K.J. De Vos, Increasing microtubule acetylation rescues axonal transport and locomotor deficits caused by LRRK2 Roc-COR domain mutations, Nat. Commun. 5 (2014) 1–11.
[83] D. Portran, L. Schaedel, Z. Xu, M. Théry, M.V. Nachury, Tubulin acetylation protects long-lived microtubules against mechanical aging, Nat. Cell Biol. 19 (2017) 391–398.
[84] Z. Xu, L. Schaedel, D. Portran, A. Aguilar, J. Gaillard, M.P. Marinkovich, M. Théry, M.V. Nachury, Microtubules acquire resistance from mechanical breakage through intralumenal acetylation, Science. 356 (2017) 328–332.
[85] A.M. Ghelli, A.M. Porcelli, C. Zanna, S. Vidoni, S. Mattioli, A. Barbieri, L. Iommarini, M. Pala, A. Achilli, A. Torroni, M. Rugolo, V. Carelli, The background of mitochondrial DNA haplogroup J increases the sensitivity of Leber's hereditary optic neuropathy cells to 2,5-hexanedione toxicity, PLoS One 4 (2009) e7922.
[86] K.R. Brunden, Y. Yao, J.S. Potuzak, N.I. Ferrer, C. Ballatore, M.J. James, A.-M.L. Hogan, J.Q. Trojanowski, A.B. 3rd Smith, V.M.-Y. Lee, The characterization of microtubule-stabilizing drugs as possible therapeutic agents for Alzheimer's disease and related tauopathies, Pharmacol. Res. 63 (2011) 341–351.
[87] Study to evaluate the safety, tolerability and the effect of BMS-241027 on cerebrospinal fluid biomarkers in subjects with mild Alzheimer"s disease, (n.d.). https://clinicaltrials.gov/ct2/show/record/NCT01492374 (accessed May 18, 2019).
[88] J.P. Dompierre, J.D. Godin, B.C. Charrin, F.P. Cordelieres, S.J. King, S. Humbert, F. Saudou, Histone deacetylase 6 inhibition compensates for the transport deficit in Huntington's disease by increasing tubulin acetylation, J. Neurosci. 27 (2007) 3571–3583.
[89] C. d'Ydewalle, J. Krishnan, D.M. Chiheb, P. Van Damme, J. Irobi, A.P. Kozikowski, P. Vanden Berghe, V. Timmerman, W. Robberecht, L. Van Den Bosch, HDAC6 inhibitors reverse axonal loss in a mouse model of mutant HSPB1–induced Charcot-Marie-Tooth disease, Nat. Med. 17 (2011) 968–974.
[90] CKD-504 in SAD and MAD in healthy Korean and Caucasian adult male and female subjects, (n.d.). https://clinicaltrials.gov/ct2/show/NCT03713892 (accessed May 18, 2019).